ENGINEERING EXPERIMENT STATION
DEPARTMENT OF MECHANICAL
AND INDUSTRIAL ENGINEERING
ME-TR-NGR-048

TRANSIENT THERMAL BEHAVIOR OF SIMPLE STRUCTURES IN A SIMULATED SPACE ENVIRONMENT BY MODEL TESTING

By

B.T. CHAO, J.S. DePAIVA, NETTO,

and

M. N. HUANG

RESEARCH ON
TRANSIENT THERMAL MODELING
OF SPACECRAFTS

NASA GRANT NGR 14-005-048

UNIVERSITY OF ILLINOIS
URBANA, ILLINOIS
JULY, 1967

ENGINEERING EXPERIMENT STATION
DEPARTMENT OF MECHANICAL
AND INDUSTRIAL ENGINEERING
ME-TR-NGR-048

TRANSIENT THERMAL BEHAVIOR OF SIMPLE STRUCTURES IN A SIMULATED SPACE ENVIRONMENT BY MODEL TESTING

by

B. T. Chao, J. S. DePaiva, Netto, and M. N. Huang

RESEARCH ON

TRANSIENT THERMAL MODELING OF SPACECRAFTS

NASA GRANT NGR-14-005-048

UNIVERSITY OF ILLINOIS
URBANA, ILLINOIS
JULY, 1967

ACKNOWLEDGMENTS

This research was supported by a NASA Grant, NGR-14-005-048, for which the authors express their appreciation.

The experimental program was behind schedule due to delay in the delivery of the space simulation chamber and, subsequently, difficulties experienced in its operation. The sympathetic understanding of Mr. Conrad Mook of NASA headquarters in Washington is sincerely appreciated.

The authors extend their gratitude to Drs. John W. Lucas, J. Michael Vickers and Curtis Rhodes of the Jet Propulsion Laboratory, Pasadena, California, for their interest, counseling and support of this research program.

TABLE OF CONTENTS

1. INTRODUCTION

At the present time, engineers have at their disposal several methods for assessing the thermal performance of a spacecraft. If the surface and bulk thermophysical properties of the materials used in the construction of the spacecraft are accurately known, if the joint conductances are predictable and if the geometric configuration is not too complicated, then analysis based on established physical laws and utilizing modern high speed computers could conceivably lead to the desired solution. Unfortunately, available information on the complex surface property of materials with respect to incident and reflected radiation of short and long wavelength is, at best, rudimentary. Our understanding of the physics of such crucial problems like thermal contact resistance, multilayer insulation, etc., is far from being adequate. Hence, purely analytical techniques have obvious limitations. An alternative would be the testing of the full scale prototype in a space simulation chamber. This has indeed been done. However, as the nation is faced with the prospect of building larger and larger spacecrafts, the high cost of constructing and operating large space simulation chambers may make prototype testing prohibitive. On the other hand, from the research and development programs undertaken by the space industry, either governmental or private, it appears that the prediction of spacecrafts' thermal performance by testing scaled-down models offers another possibility.

While the theoretical requirements and the basic modeling criteria have been extensively studied and reasonably well understood, the practical implementation of satisfying the criteria must be considerably advanced from what is known today if the modeling technique were to be competitive with others. It is our belief that its success or failure would depend, to a large extent, on the engineer's ability to recognize and distinguish the significant variables from the unimportant ones, to introduce simplifications and to develop correction procedures for imperfect modeling.

In a recent 'state-of-the-art' report on a study carried out by the Jet Propulsion Laboratory, California Institute of Technology, Vickers [1]*

*Numbers in brackets refer to References at end of this Report.

stated: "A half-scale thermal model can be built in a time period consistent with spacecraft development which, from ground test, can give steady-state predictions to an accuracy which is of value in the thermal control of the flight prototype. More development is needed to prove that the same type of accuracy can be attained when predicting the transient behavior of spacecraft." As a step to fulfill such need and to achieve the above stated objective, we have set forth, first, to conduct transient modeling experiments on relatively simple structures under both strongly and weakly radiation-conduction coupled conditions. A prototype, a $\frac{1}{2}$-scale and a $\frac{1}{4}$-scale model, each consisting of two different materials arranged to give three geometric configurations were partly built and tested. Available results indicate that our original concept of artificially controlling the thermal conductivity by electroplating and the use of thickness distortion for plate-type structural members to satisfy transient modeling criteria are feasible.

2. BRIEF LITERATURE REVIEW

Vickers [2] gave an excellent review of literature on thermal modeling of spacecrafts published up to 1965, with description of research and development work in progress at that time. He pointed out the uses and advantages of testing scaled models as well as problems which needed solution, particularly for transient modeling. A comprehensive survey of the subject, with emphasis on the mathematical theory of dimensional analysis and similitude as applied to thermal design of spacecrafts has been given by Jones [3]. A recent lecture series presented by Gabron [4] at the University of California in Los Angeles contained an annotated bibliography of 31 papers available in open literature. In view of these, there is little need for compiling another bibliography on thermal scale modeling at the present time. Instead, we shall only briefly review several publications in which results of model testing involving nonsteady heat flow phenomenon were reported.

Adkins [5] presented the results of measurement of transient temperatures of a hollow, thin-wall cylinder and sphere, heated by radiation from an adjacent flat plate in a cold wall vacuum chamber. The test objects were physically isolated from one another and were fabricated of one homogeneous

material. The model was of $\frac{1}{2}$-scale with distorted thickness to satisfy similitude requirements. A second configuration consisting of two hollow, stainless steel spheres connected by a copper rod was also studied. One of the spheres was internally heated, and heat transfer between them took place by conduction along the rod in addition to the radiant exchange. Data were reported for "average" temperatures only. At homologous locations and times, the prototype and model temperatures agreed to within approximately 20°F. Experiments similar to Adkin's first configuration were also conducted by Jones and Harrison [6]. The temperatures were monitored by a large number of thermocouples installed in the cylinder, the sphere and the flat plate. Heat exchange among the objects was by radiation only. In general, the results were satisfactory except for certain locations where the model temperature deviated considerably from the corresponding prototype temperature. Explanations were offered for the observed discrepancy. It was pointed out that care should be exercised to obtain proper initial conditions if model experiments were used to deduce information on periodic temperature transients. As we shall see later, the prediction of the transient thermal behavior of systems by model testing is relatively less difficult if radiation alone dominates the mode of heat transfer.

A series of thoughtful experiments on transient modeling had been conducted by Rolling [7]. Two geometric configurations were studied, one consisted of two opposed discs, representative of an open structure, and another was a truncated cone, providing a largely closed system. The $\frac{1}{2}$-scale model was designed on the basis of "material preservation" technique and the $\frac{1}{4}$-scale model was based on the "temperature preservation" technique. Two heating sources, capable of being operated independently, were employed. One was an electrical heater encased within a box and the other was from an array of tungsten filament lamps which provided incident radiation to the test object. A large number of thermocouples were installed at various locations. For the opposed disc configuration, which was tested during the initial phase of the program, errors in steady state results amounted to 5 to 10°K with a maximum of 19°K which occurred at one location of the $\frac{1}{2}$-scale model. Improved accuracy was obtained for the truncated cone configuration for which the model temperatures were generally within 5°K

of the corresponding prototype temperatures. This was attributed to the improvement in model construction, instrumentation and chamber operation as a result of the experience gained during the initial phase of the research. It was pointed out that geometric distortion in regions of high heat flux could result in serious errors. A major simplifying factor in the design of Rollings's experiments is that the test object was fabricated of one material.

Miller and Wiebelt [8] conducted transient modeling experiments using solid cylindrical rods and the conditions selected were such that heat flow was one-dimensional. In the first test series, the rods were of a single material (2024 aluminum). In the second test series, the rods were made of two cylindrical bars of practically identical diameter but different materials (2024 aluminum and 316 stainless steel) soldered end to end. The transfer of heat from the aluminum portion of the rod to the stainless steel portion was by conduction only. No radiant exchange occurred between them. The model geometry was grossly distorted so that temperatures could be preserved. It was claimed that no predicted prototype temperature was more than 13°F in error and the great majority of them were consistently less than 5°F in error. For the specific geometric and heat flow configuration selected by Miller and Wiebelt for study, modeling technique using simultaneous preservation of material and temperature is indeed attractive. Unfortunately, such highly specialized conditions seldom prevail in today's spacecraft.

In addition to the foregoing, nonsteady modeling experiments aimed at providing information for the thermal design of spacecrafts have also been reported by Folkman et al [9] and by Young and Shanklin [10].

3. MODELING CRITERIA AND DESIGN PROCEDURE

As stated under the introductory section of this report, modeling criteria for unmanned spacecrafts, for which the modes of heat transfer are dominated by radiation and conduction, have been extensively studied and reasonably well understood. Based on a detailed analysis of a general structural and thermal system with temperature dependent properties and non-gray surfaces, Chao and Wedekind [11] obtained a comprehensive list of

similarity parameters. It was found that the accuracy of modeling employing temperature preservation technique could be improved by using materials exhibiting similar temperature dependency. It was also shown that if the temperature field was two-dimensional, considerable advantage could be obtained by using models of distorted thickness. When identical materials were used for the corresponding members of the prototype and of the model, the model would operate at higher temperatures.* If model testing were to become a useful tool for the thermal design of future spacecrafts, it is most likely that models much smaller than $\frac{1}{2}$-scale may have to be built. For a prototype operating at 240°F, the corresponding 1/5 - scale model using material preservation technique would operate at 737°F. One thus encounters all the adverse effects associated with such operation, such as dimensional instability and warpage, deterioration of surface coatings, increasing difficulty of measuring large temperature gradients in small models, etc. If solar simulation is involved, the spectral intensity needs to be scaled in proportion to the fourth power of the ratio of model to prototype temperatures. For all these reasons, temperature preservation technique has been adopted in the present investigation. However, it is pertinent to reiterate what Rollings [7] has already emphasized, "The model criteria in themselves do not dictate a specific model test procedure . . . (Their) full utility can be realized for a particular study by (recognizing) their complete flexibility . . . To select a preservation technique before careful consideration of other approaches will often place initial restrictions on the study which result in unnecessary difficulties."

To facilitate further discussion, we list first the nomenclature and then the similitude requirements for transient modeling of systems with two-dimensional heat flow using temperature preservation technique.

3.1 Nomenclature

C = volumetric heat capacity, product of specific heat and density

d = thickness

*Only in certain special configuration such as the one studied in [8], this requirement could be relaxed.

L = characteristic length

k = thermal conductivity

q = heat flux

t = time

T = absolute temperature

ϵ = emittance

Subscripts:

b refers to base material

i refers to surfaces in the system. In the present phase of investigation, i = 1, 2. It also refers to materials used for fabricating the surfaces.

p refers to thermal paint

ep refers to electroplating

* refers to model

(Quantities with an overscore denote equivalent values.)

3.2 Transient Modeling Criteria

The following is adapted from [11], taking into consideration of the fact that, in this phase of research, solar simulation is not involved and the prototype and model surfaces are coated with the same thermal paint.†

Model geometric scale

$$\left(\frac{L^*}{L}\right)^2 = \frac{k_i^* d_i^*}{k_i d_i} \qquad (1)$$

Model time scale

$$\frac{t^*}{t} = \frac{C_i^* d_i^*}{C_i d_i} \qquad (2)$$

---

† This does not necessarily guarantee that the surface emittance will be precisely identical. Small variations in ϵ had been repeatedly noted even though a seemingly identical spraying and drying procedure were used. Furthermore, the emittance of the painted surface changed somewhat after prolonged testing, possibly due to contamination by the vacuum oil vapor in the chamber. A procedure to partially overcome such difficulty will be explained later.

In Eqs. (1) and (2), both the thermal conductivity and heat capacity are taken as average values. The conductivity of the six materials used in the fabrication of the prototype and the models was measured in the Heat Transfer Laboratory of the University. Details of the experimental apparatus, method of specimen preparation and results are given in Appendix 1 of this report. All but Nickel-L (one of the two metals used in the $\frac{1}{4}$-scale model) showed some increase in conductivity with temperature. In the current series of tests, the local temperatures of the test object ranged from approximately 540°R to 780°R with a mean of 660°R. Within this temperature range, the maximum deviation of the local conductivity from its mean ranged from less than 1% for EC - aluminum to slightly above 9% for aluminum bronze (copper alloy 614).

The specific heat of the materials has not been measured but was calculated from the chemical composition using the Neumann-Kopp rule. The method of computation and the results are presented in Appendix 3. The volumetric heat capacity of all six materials increases with increase in temperature. Within the above stated temperature range, the maximum deviation from the mean amounted to 1.6% for aluminum bronze (copper alloy 614) and 6.7% for Nickel-L with others falling between these extremes. At the present time, no successful theory has been developed to predict the effect of such variations in conductivity and heat capacity on modeling accuracy.

When the system to be modeled consists of more than one material, which is invariably the case for actual spacecrafts, the simultaneous satisfaction of criteria (1) and (2) for all component surfaces is not usually possible if commercially available metal sheets or plates are used. As suggested in our original proposal, one possibility of overcoming such difficulty is to use composite plate or sheet produced by electroplating. Referring to Fig. 1, there is shown schematically a base plate of thickness d_b^* with electroplated layer on both surfaces of total thickness d_{ep}^* and thermal paint coating of total thickness d_p^*. The equivalent $\overline{k^* d^*}$ and $\overline{C^* d^*}$ of such composite metal sheet are respectively given by:

$$\overline{k^* d^*} = k_b^* d_b^* + k_{ep}^* d_{ep}^* + k_p^* d_p^* \qquad (3)$$

and

$$\overline{C^* d^*} = C_b^* d_b^* + C_{ep}^* d_{ep}^* + C_p^* d_p^* \qquad (4)$$

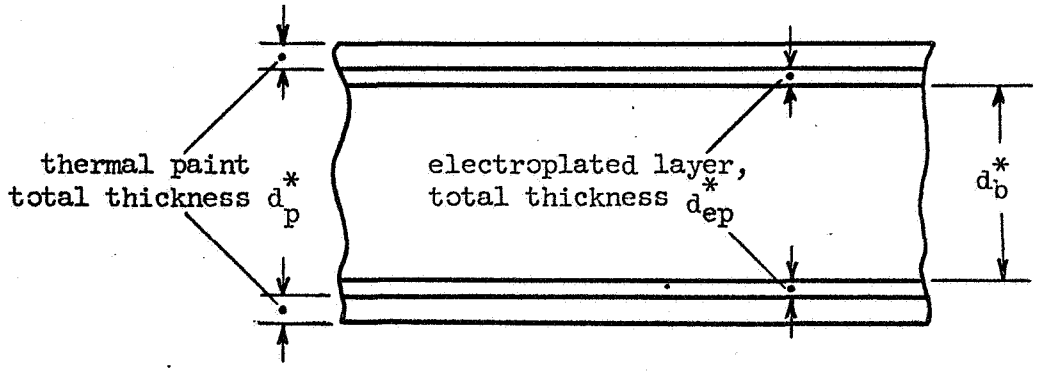

Fig. 1 Composite Metal Sheet Used in Model Construction

Similar expressions could be written for the prototype. By a judicious selection of the base material and the metal to be plated, it is possible to satisfy both modeling criteria (1) and (2) for all different members of the system. Practical considerations for the selection are: the availability of the materials, ease of fabrication, degree of sophistication of the electroplating facility required, etc.

3.3 Modeling Design Procedure

3.3.1 General Discussion

The design starts with the aim of satisfying the modeling criteria for the most abundantly used material in the system, or for those surfaces which essentially control the system thermal performance. These will be designated as material ①. In accordance with the first criterion given in the previous section, we require:

$$\left(\frac{L^*}{L}\right)^2 = \frac{k_{1,b}^* d_{1,b}^* + k_{1,p}^* d_{1,p}^*}{k_{1,b} d_{1,b} + k_{1,p} d_{1,p}} \qquad (5)$$

Since the same thermal paint is used for the prototype and the model, $k_{1,p}^{*} = k_{1,p}$. If bare material is employed, the second term in both the numerator and denominator should obviously be deleted. In a great majority of cases, the contribution of paint conduction is very small and can be neglected. The model base material and its thickness are so chosen that $\frac{L^*}{L}$ is close to what is desired. The principal limiting factor is the availability of commercial stock of metal plates or sheets. Obviously, there is no need for the geometric scale ratio being an integer.

Having selected the material and the thickness, the model time scale is fixed. It is given by:

$$\frac{t^*}{t} = \frac{C_{1,b}^{*} d_{1,b}^{*} + C_{1,p}^{*} d_{1,p}^{*}}{C_{1,b} d_{1,b} + C_{1,p} d_{1,p}} \quad . \qquad (6)$$

As in the case of conductivity, the contribution to the overall heat capacity due to the thin coat of thermal paint is usually very small.

For other materials or surfaces in the system, our scheme to satisfy the modeling requirements is to use composite plates fabricated by electroplating as has already been mentioned. In what follows, they will be designated as material ②.† Hence, for the latter, we would require:

$$\frac{k_{2,b}^{*} d_{2,b}^{*} + k_{2,ep}^{*} d_{2,ep}^{*} + k_{2,p}^{*} d_{2,p}^{*}}{k_{2,b} d_{2,b} + k_{2,p} d_{2,p}} = \left(\frac{L^*}{L}\right)^2 \qquad (7)$$

and

$$\frac{C_{2,b}^{*} d_{2,b}^{*} + C_{2,ep}^{*} d_{2,ep}^{*} + C_{2,p}^{*} d_{2,p}^{*}}{C_{2,b} d_{2,b} + C_{2,p} d_{2,p}} = \frac{t^*}{t} \quad . \qquad (8)$$

In (7) and (8), the right hand side has already been prescribed. The selection of thermal paint is usually dictated by prototype thermal design conditions. Since copper has a conductivity higher than any other metals

---

† The discussion given here is directly applicable to materials ③, ④, etc., if they are present.

except silver and the technology of electroplating copper has been quite well developed, it was chosen in the present investigation.

A question which arose and needed to be answered was concerned with the thermal conductivity of the electrodeposited copper. It has been known that the physical and thermal properties of metals prepared by electrodeposition may be different from the properties of the same metal in the cast or rolled state. The deposited metals usually appear to be in a state of internal strain. Their appearance under the microscope varies widely with materials; the grain size is also influenced by the rate and conditions of deposition. It was thus decided to measure the thermal conductivity of the electroplated copper. The procedure and the results are given in Appendix 2.

3.3.2 Material Selection

In the thermal modeling of actual spacecrafts, the prototype materials are prescribed; they are selected from mission requirements. For the purpose of present investigation, we have arbitrarily chosen a high conductivity metal--EC - aluminum--and a medium conductivity metal--aluminum bronze (copper alloy 614). Originally, ARMCO iron was chosen for the latter but we were forced to abandon the choice due to the supplier's unwillingness to deliver a small quantity for our use.

The main thermophysical property governing the selection of model material is thermal conductivity because it is directly related to the geometric scale and because it has a wide range of variation, of the order of 1 to 20 or more, among commercially available metals and alloys. In contrast, the volumetric heat capacity shows a much smaller variation, usually within a ratio of 1 to 2 or 3. It is directly related to the model time scale which is ordinarily not prescribed.

The first step in model material selection was to compile data on thermal conductivity and specific heat of metals and alloys from published literature. For the metal alloys, the dearth of adequate information on conductivity was immediately felt; most sources gave data only for one temperature, usually the room temperature. Discrepancies among different sources are also not uncommon. While it was decided during the very early

stages of the present research program to measure the conductivities in our own laboratory, this could not be pursued without first deciding on materials used for the prototype and the models. The results of our initial literature search were displayed in Fig. 2 in which the thermal conductivities of five groups of metals and alloys are plotted against their heat capacities. Of interest is the fact that each group occupies a rather limited region in such a plot. This observation was utilized in the choice of material by a computer program as explained below. Referring to the similarity requirements (7) and (8), it is seen that the unknowns in the two equations are $k^*_{2,b}$, $C^*_{2,b}$, $d^*_{2,b}$, and $d^*_{2,ep}$. For an assigned material, $k^*_{2,b}$ and $C^*_{2,b}$ become known and the two remaining unknowns, $d^*_{2,b}$ and $d^*_{2,ep}$ can be determined. This was done on the computer using a program whose input contained the thermal property data of 20 to 25 metals and alloys. The availability of the material in plate or sheet form and the information given in Fig. 2 serve as a guide in their choice for study. Another limitation incorporated in the computer program was that the thickness of the electroplated copper* should not exceed 0.003 inch. It was found that a number of possible combinations of materials and thicknesses existed. As it turned out, a severe limiting factor which dominated the final choice was the reluctance on the part of many metal suppliers to consider small orders. In other instances, the undue long delivery time nullifies the consideration.

The thermal conductivities of all the materials used in the prototype and model construction were carefully measured over the design temperature range in our own laboratory for reasons given earlier. Their heat capacities were calculated from the known chemical composition using the Neumann-Kopp rule. An average was then determined for both the conductivity and heat capacity and entered into the computer program for the more accurate, final evaluation of the base metal thickness $d^*_{2,b}$ and plating thickness $d^*_{2,ep}$.

4. SYSTEM CONFIGURATIONS; GEOMETRIC AND TIME SCALE OF THE FABRICATED MODELS

The main objective of the first phase of the experimental program was to investigate the feasibility of artificially modifying the thermal proper-

---

*Earlier, metals other than copper were also investigated by the same computer program. We soon came to the conclusion that copper was the best choice, taking into account all the factors involved.

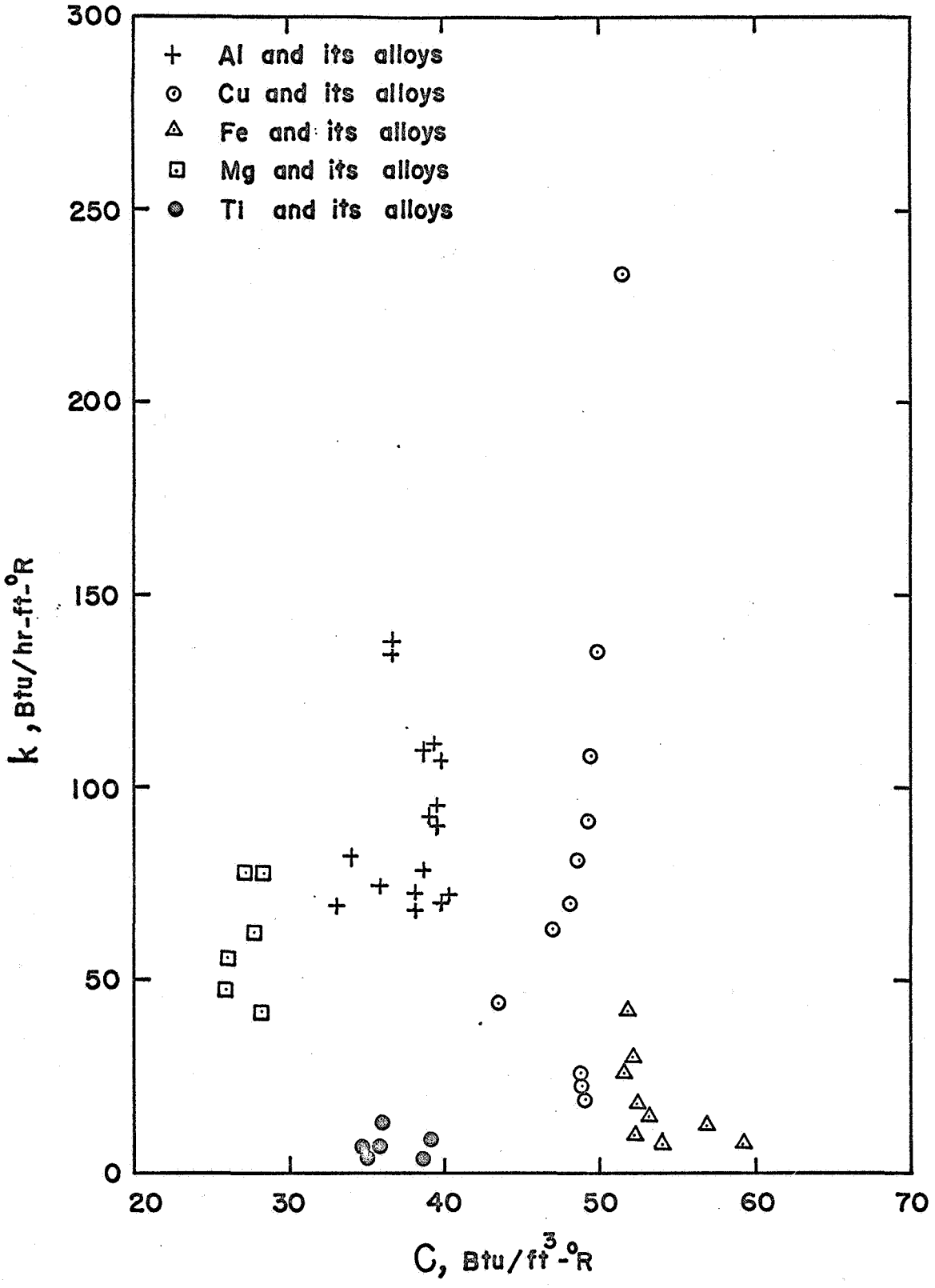

FIG. 2 RANGE OF THERMAL CONDUCTIVITY AND HEAT CAPACITY OF SEVERAL METALS AND ALLOYS

ties of metal plates or sheets by electroplating in order that the transient modeling requirements of systems involving more than one material could be satisfied. A rather simple geometric configuration was selected so that the test results might shed light on the nature of modeling errors, and, hence, eventually lead to the development of a technique of approximate modeling with error correction. Fig. 3 depicts the simplest configuration in which the two surfaces of the structure have negligible radiative exchange. Major dimensions of the prototype and the models, thickness of electrodeposited copper, thermocouple sizes and locations, etc., are all shown. The various thicknesses listed are measured values; they deviate somewhat from the theoretical requirements. With the modest electrodeposition facility which was available for our use, it was rather difficult to hold the plating thickness within close limits. Its uniformity was somewhat less than desired. There were also some minor inaccuracies in the thickness of base metal sheets.

A preliminary study was made to search for a satisfactory procedure for installing the thermocouples. Details are described in Appendix 4. It cannot be overemphasized the importance of observing the recommended procedure in every instance.

A total of ten holes was provided for bolting together the plates and the electrical resistance heating element sandwiched in between. The bolts used for the prototype and for the models were approximately scaled but not thermally similar due to availability. For this reason, their stems and heads were insulated from the plates to reduce conduction errors. The metal plates for the prototype and the $\frac{1}{2}$-scale model were finished to their final dimensions in a surface grinder, using a specially designed grinding fixture. A number of countersunk holes were drilled (not shown in Fig. 3 for clarity) for securing the plates onto the grinding fixture. They were all properly scaled. At the neighborhood of their holes, the overall one-dimensional heat flow pattern in this simple configuration was disturbed.

According to our concept of model design as described in Section 3, only one of the model material need be plated. Due to mistakes made in gaging the plate thickness during grinding, it was found necessary to electroplate both the 5086 aluminum and the 65-15 nickel silver plate of

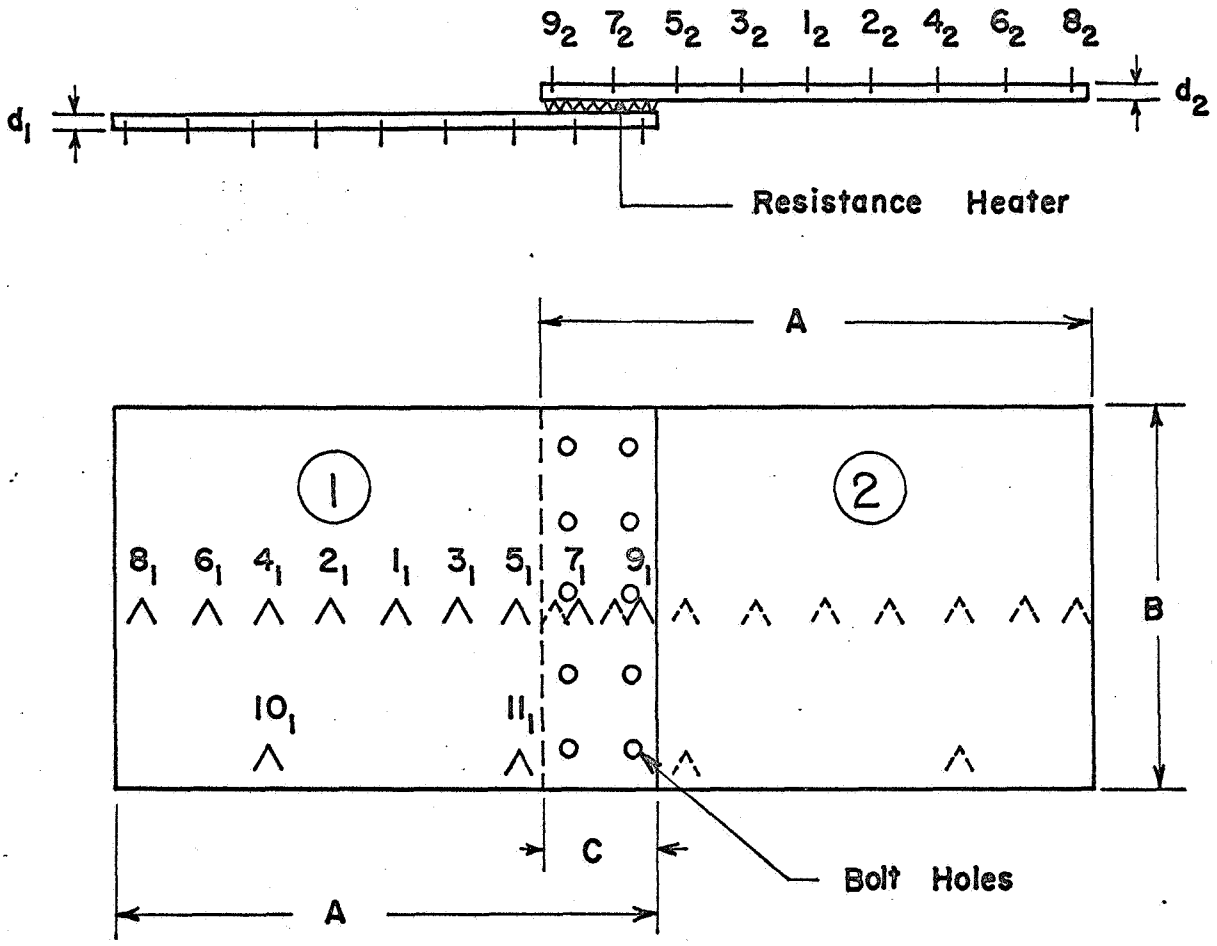

∧ Designate thermocouple location

All surfaces are spray-painted with 0.002 in Thermokote Aluminum 625

FIG. 3 MODEL CONFIGURATION (a)

		Prototype	1/2 - Scale Model	1/4 - Scale Model
Material	①	EC - Aluminum	5086 Aluminum-Magnesium alloy	Nickel L
	②	Aluminum-Bronze (Copper alloy 614)	65-15 Nickel silver (Copper alloy 754)	304 stainless steel
Base Metal Dimensions, in.	A	20	10	5
	B	14	7	3.5
	C	4.5	2.25	1.125
	d_1	.2905	.1177	.0559
	d_2	.2038	.0767	.0600
Thickness of Electroplated Copper, in.	$d_{1,ep}$	———	.00045	.00085
	$d_{2,ep}$	———	.00279	———
Bolt Hole in.		.147	.109	.043
Iron-Constantan Thermocouple		AWG 24	AWG 30	AWG 36

LEGEND FOR FIG. 3

the $\frac{1}{2}$-scale model. This, however, has no bearing on the basic objective which we set forth to investigate.

In addition to the configuration described above, two additional system configurations have also been selected for study. They are shown in Fig. 3-1. Configuration (b) is similar to (a) except that there is a significant radiation exchange between the two surfaces. The slot cut in each of the plates of Configuration (c) is to produce a distinct two-dimensional temperature field. At the time when this report was in preparation, test results for the latter two configurations have not been completed. However, they will be presented in the Semi-Annual Technical Report to be submitted to the Jet Propulsion Laboratory of Pasadena, California, later this year. JPL has continued to support this research when the initial one-year funding from NASA was exhausted.

The heat capacity of the electric resistance heaters was approximately scaled according to the model time scale. Details of their construction and electrical data are shown in Fig. 4. Since accurate power measurement is of prime importance, every effort was made to reduce possible errors. All heaters were designed to operate with relatively low current and high voltage, compatible with a commercially available d.c. power supply.

Using the measured properties and thicknesses of the finished metal sheets and those of the plating and paint layers, the geometric and time scale of the models were calculated. The precise variation of thermal conductivity and heat capacity with temperature was not considered, instead, their averages evaluated at the estimated mean temperature of 660°R were used. The conductivity and heat capacity of the "Thermokote" aluminum paint were not known but estimated to be 0.1 Btu/hr-ft-°R and 20 Btu/ft^3 - °R respectively. All paint layers had a thickness of approximately 0.002 inch - 0.0025 inch. As can be seen from Table I, the paint has negligible contribution to the overall conductance. On the other hand, the contribution of the plated copper is significant but its effect on overall heat capacity is small.

The geometric and the time scale of the models can be easily calculated using the values of $\overline{kd}$ and $\overline{Cd}$ listed in Table I. The results are given in Table II. The small discrepancies (up to approximately 1%) which existed in the scale ratios are due to minor deviations in thick-

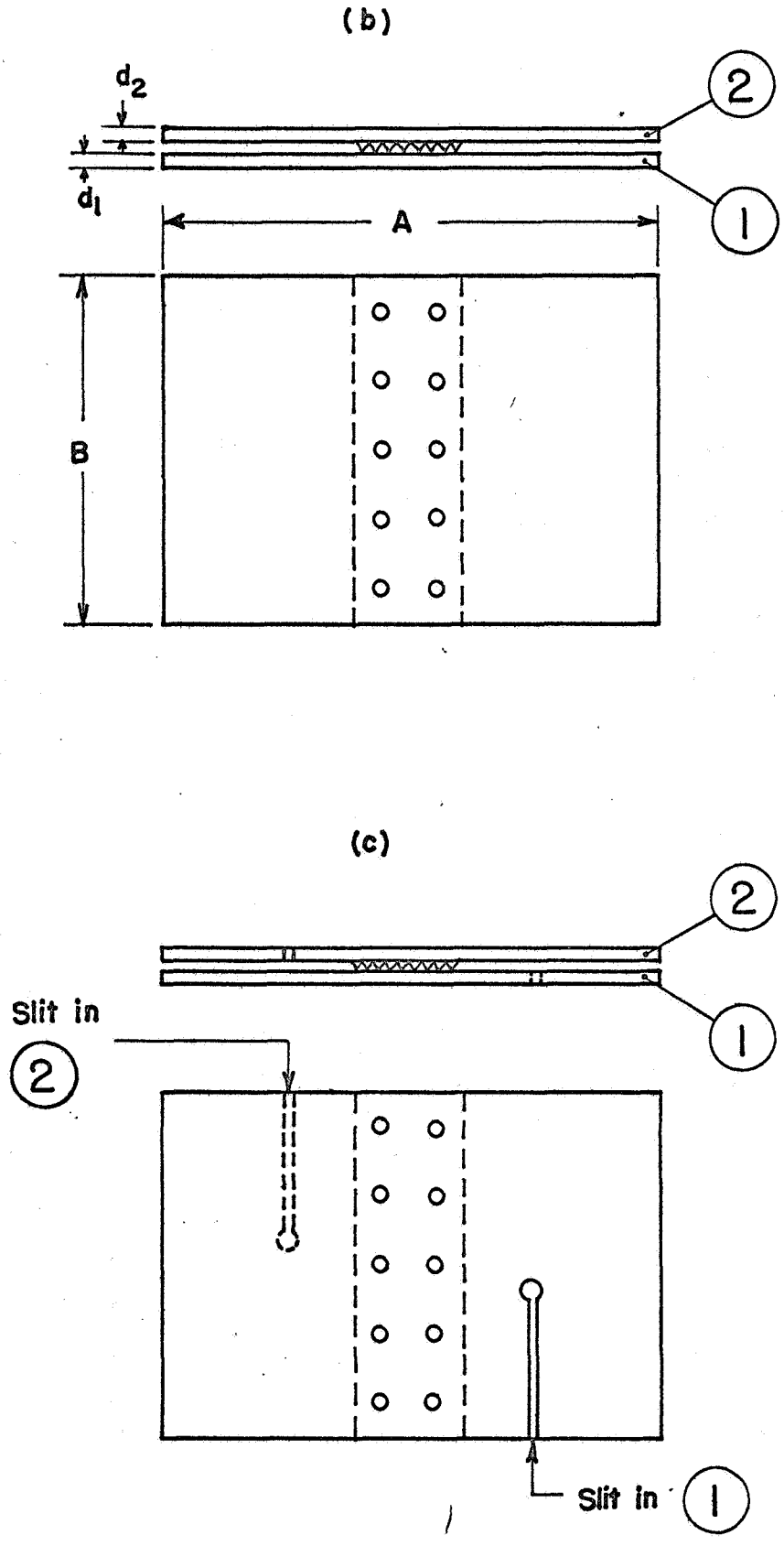

FIG. 3-1 MODEL CONFIGURATIONS (b & c)

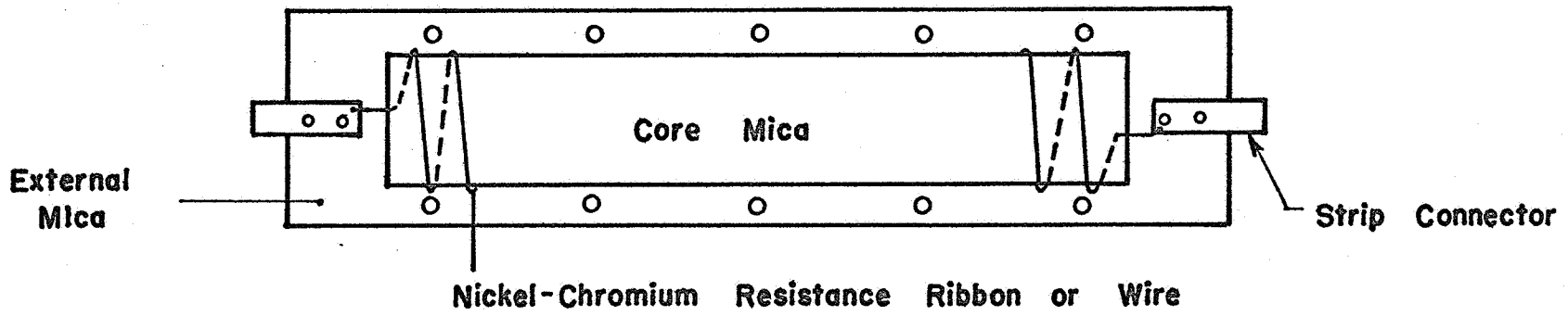

	Prototype	$\frac{1}{2}$-Scale Model	$\frac{1}{4}$-Scale Model
	.004" ribbon 5-layers	.007" wire 3-layers	.003" wire 3-layers
Total Thickness in. — Mica	.070	.030	.015
Total Thickness in. — Heating Element	.016	.014	.006
Maximum Power	460 W. at 320 V.	115 W. at 230 V.	28.8 W. at 144 V.
Resistance, ohm	215	415	650

FIG. 4 DETAILS OF ELECTRICAL STRIP HEATER

TABLE I. EQUIVALENT $\overline{kd}$ AND $\overline{Cd}$ OF SYSTEM COMPONENTS

		kd			$\overline{kd}$	Cd			$\overline{Cd}$
		base metal	electro-plating	paint		base metal	electro-plating	paint	
Prototype	Material ① EC-Aluminum k = 132.6, C = 37.7	38.52	--	.0004	38.52	10.96	--	.10	11.06
	Material ② Aluminum-Bronze (Copper Alloy 614) k = 41.2, C = 50.6	8.40	--	.0004	8.40	10.31	--	.10	10.41
$\frac{1}{2}$ - Scale Model	Material ① 5086 Aluminum-Magnesium Alloy k = 80.2, C = 37.1	9.44	.099	.0004	9.54	4.37	.023	.08	4.47
	Material ② 65-15 Nickel Silver (Copper Alloy 754) k = 19.2, C = 52.4	1.47	.612	.0004	2.08	4.02	.145	.08	4.25
$\frac{1}{4}$ - Scale Model	Material ① Nickel-L k = 40.5, C = 62.8	2.26	.187	.0004	2.45	3.51	.044	.08	3.63
	Material ② 304 Stainless Steel k = 8.9, C = 56.3	.534	--	.0004	.534	3.38	--	.08	3.46

k in Btu/hr-ft-°R, C in Btu/ft^3-°R, kd in Btu-in/hr-ft-°R, Cd in Btu-in/ft^3-°R

TABLE II. GEOMETRIC SCALE AND TIME SCALE OF MODELS

	Based on Material ①	Based on Material ②
(A) Prototype vs $\frac{1}{2}$ - Scale Model:		
$\frac{L^*}{L}$	$\sqrt{\frac{9.54}{38.52}} = \frac{1}{2.01}$	$\sqrt{\frac{2.08}{8.40}} = \frac{1}{2.01}$
$\frac{t^*}{t}$	$\frac{4.47}{11.06} = .404$	$\frac{4.25}{10.41} = .408$
(B) Prototype vs $\frac{1}{4}$ - Scale Model:		
$\frac{L^*}{L}$	$\sqrt{\frac{2.45}{38.52}} = \frac{1}{3.97}$	$\sqrt{\frac{.534}{8.40}} = \frac{1}{3.97}$
$\frac{t^*}{t}$	$\frac{3.63}{11.06} = .328$	$\frac{3.46}{10.41} = .332$
(C) $\frac{1}{2}$ - Scale Model vs $\frac{1}{4}$ - Scale Model		
$\frac{L^*}{L}$	$\sqrt{\frac{2.45}{9.54}} = \frac{1}{1.97}$	$\sqrt{\frac{.534}{2.08}} = \frac{1}{1.97}$
$\frac{t^*}{t}$	$\frac{3.63}{4.47} = .812$	$\frac{3.46}{4.25} = .814$

ness of the base metal sheet and of the copper plating from the theoretical values.

5. EXPERIMENTAL FACILITIES, DATA RECORDING SYSTEM AND TEST PROCEDURE

5.1 Space Simulation Chamber

The vacuum chamber was fabricated by the AVCO Instrument Division of Tulsa, Oklahoma, in accordance with our specifications. It consists of three major subsystems--a chamber with liquid nitrogen cooled shroud, a pumping system and a control system.

The chamber is in the form of a horizontal cylinder, approximately 42 inches in diameter and 48 inches long with flanged and dished heads. One of the heads is seam-welded to the end of the cylinder and the other is used as a door. Toward the open end of the cylinder and on the side is an instrument port for thermocouple and power lead feedthroughs.

Contained within the cylindrical chamber is a LN_2 shroud which is of "Platecoil" structure consisting of a cylindrical section with two flat end panels. The liquid nitrogen is supplied from a standard 80 liter dewar. One of the end panels is mounted in the door dish head and has a separate line for feeding LN_2. The shroud temperature varied over a wide range, -315°F near the bottom to -230°F near the top. The difference can be reduced by flooding it with LN_2 but it has been found unnecessary for the purpose of the present experiments. The inner surface of the shroud was painted with Cat-A-Lac black, producing an emittance of 0.9 or better. Its outer surface was polished to give a low emittance which the supplier claimed to be 0.1 or less.

The pumping system consists of a Welch 1398 mechanical pump for roughing and backing a Consolidated Vacuum Corporation PMC-10B diffusion pump. The mechanical pump has a rated capacity of 50 cfm and the diffusion pump is rated at 4100 liters per second. The pumping system is connected to the chamber through a ten-inch pneumatically actuated gate valve. A three-inch gate valve connects the mechanical pump and the diffusion pump and another three-inch gate valve is installed between the mechanical pump

and the chamber. These valves allow the chamber to be roughed and the diffusion pump to be backed as directed from the control system. A small vent valve is provided to repressurize the chamber.

The control system is semi-automatic and the status of all valves, pumps, motors, etc., is indicated by lamps on a control panel. Start, rough, run or vent is selectable from switches. Certain valve operations are sequenced with other operations, for example, the backing valve can be open only after a certain time of rough pumping to prevent over pressurizing the diffusion pump. These are made possible by timers controlled by limit switches.

Included in the panel is a circuit breaker section for electrical equipment failure protection. Also included is a vacuum gaging system. The latter consists of two Pirani gauges and a hot-filament ionization gauge (CVC, Type GIC-111). The Pirani gauges are for monitoring roughing and backing pressure in the micron ranges and the ionization gauge is for measuring chamber pressure in 10^{-7} torr range. During all tests, the chamber pressure was maintained approximately at 5×10^{-7} torr. At this level of vacuum, convective effects are known to be negligible.

The flow of LN_2 into the shroud is controlled by a thermistor sensor, a relay and a potentiometer in series. When the thermistor is warm, its resistance is low and current is drawn through the relay. The energized relay turns on the current to a magnetic valve, allowing the flow of LN_2. When the LN_2 level reaches the sensor, there is a sharp increase of the thermistor resistance, thus reducing the relay current which, in turn, would close the valve. In the present series of experiments, this automatic control was not actually used as it resulted in an excessive consumption of LN_2. Instead, the on and off switch for the magnetic valve was controlled manually and this was guided by the five thermocouple readings attached to the shroud.

5.2 Power Supply and Power Measurement

The d.c. current for the resistance heater was from a regulated power supply manufactured by the Harrison Laboratories of New Jersey. It provides

a continuously adjustable output, ranging from 0-320 volts and 0-1.5 amperes. When the line voltage fluctuates between 105 and 125 volts, the regulation of the power supply remains less than .007% in output voltage practically for the entire range from no load to full load. Its drift has been found negligible after suitable warming up period.

During the early stages of experimentation, the voltage and current supplied to the heater were measured with a multirange d.c. voltmeter and ammeter of 0.35% full scale precision. Improved results were later achieved by using a Leeds and Northrup precision volt box and shunt box in conjunction with an L & N potentiometer. Both the volt and shunt box have a claimed accuracy of ±0.02%. With the latter scheme, the error in power measurement has been estimated to be less than 0.2%.

5.3 Data Recording Systems

The output of the eleven thermocouples installed on each material of the test object was continuously monitored by two Leeds and Northrup, 12-point, adjustable zero, adjustable range strip chart recorder. The thermocouples have individual cold junctions maintained at 32°F in a stirred ice bath. These recorders provided a visual indication of the thermal behavior of the system under study--approaching steadiness, response to an adjustment of heater power, etc. However, it was found somewhat time consuming to read the chart and replot the data. Subsequently, an automatic data acquisition system with digital printout was procured. It is highly successful in that it not only facilitates the data processing but also eliminates human error in chart reading. However, due to limitation in available fund and the long delivery time, the present system is only capable of handling ten thermocouple readings.

This digital printout system consists of a scanner, a digital millivoltmeter with binary coded output, a digital clock, a multiplexing unit and, finally, a printer. Fig. 5 shows schematically the arrangement with an actual sample of the printout tape. The left column on the tape gives the thermocouple identification number, while their output in millivolts is printed in the right column. The first reading in the left column of each group also gives the time. The time interval between the successive print-

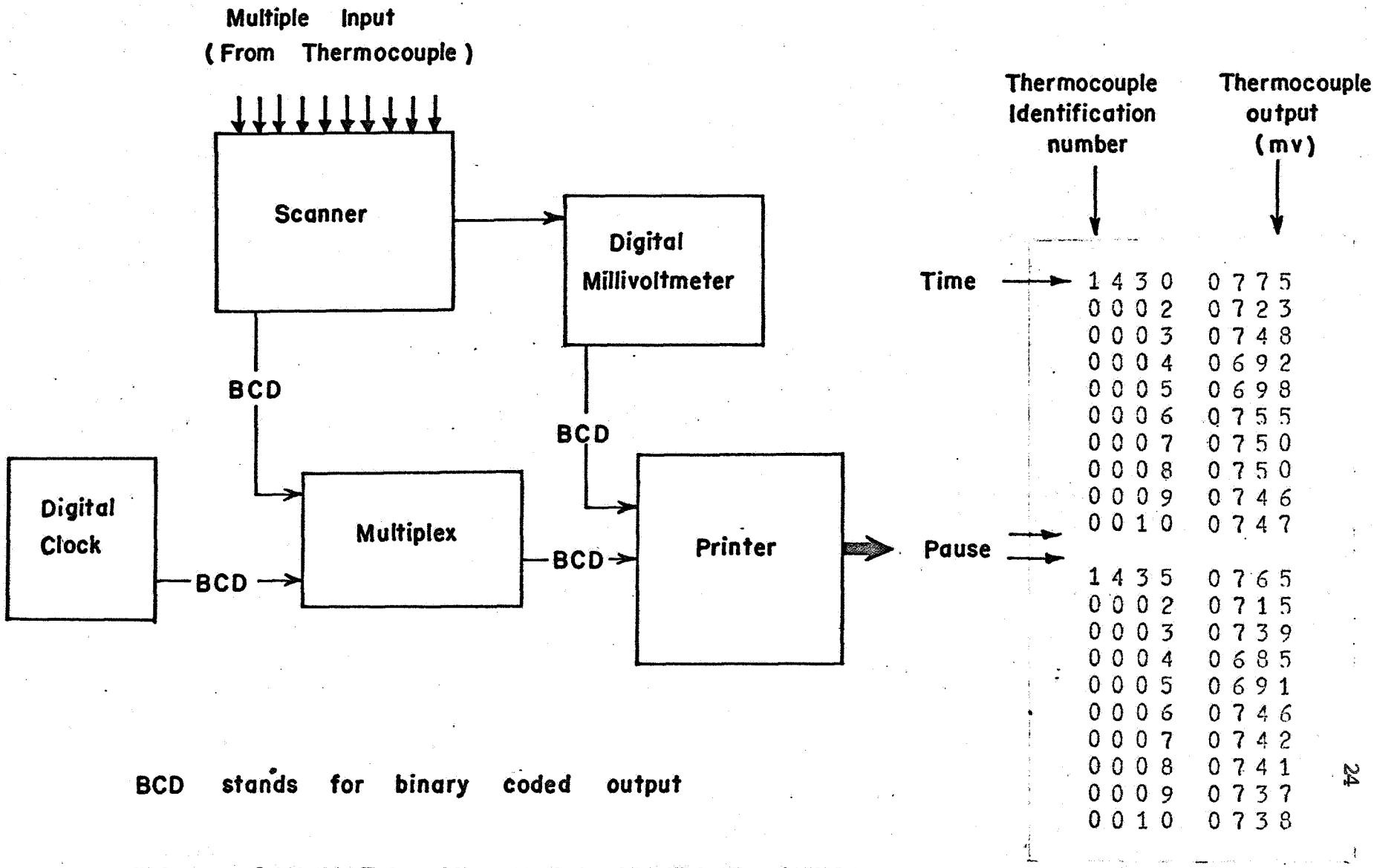

BCD stands for binary coded output

FIG. 5 SCHEMATIC OF DIGITAL PRINTOUT SYSTEM

outs is adjustable from 0.1 second to 10 seconds. In actual operation, the response time of the digital millivoltmeter usually governs the selection. The scanner could be operated either manually or in continuous cycles with data printed out every 1 minute, 5 minutes, etc.

The accuracy of the system is completely governed by that of the digital millivoltmeter. The manufacturer claimed an accuracy of 0.1% of full scale reading ±10 μv which amounted to a maximum error of 20 μv or approximately 2/3 °F in our application. The instrument was checked in our laboratory against a Leeds and Northrup precision potentiometer and was found to have an accuracy approximately twice the stated value when it was new. However, its accuracy deteriorated somewhat after a continuous usage of a few months.

The output of the five thermocouples welded to the LN_2 shroud was also measured by a digital voltmeter through a manually operated rotary selector. These were not continuously recorded.

5.4 Test Procedure

The test object was suspended in the chamber using insulated thermocouple wires of the same gage as that for temperature measurement. Prior to the actual test run, all thermocouples were examined for possible defects in installation by examining their responses as the test object was heated and cooled in still air. In a few instances, replacement was found necessary. The orientation of the test object was such that the rectangular plates were vertical with their long sides running parallel to the horizontal axis of the cylindrical chamber as is illustrated in Fig. 6. To ascertain the influence of the instrument port on the surface radiation transfer of the test object, two tests were conducted for the prototype--one with the EC - aluminum plate directly facing the port and another with the aluminum bronze plate facing the port by turning the test object 180° about its vertical axis. No significant difference in the steady-state temperature distribution was found. Similar tests were not made for the $\frac{1}{2}$-scale and $\frac{1}{4}$-scale models since they were located toward the rear of the shroud and hence the influence of the instrument port was decidedly less.

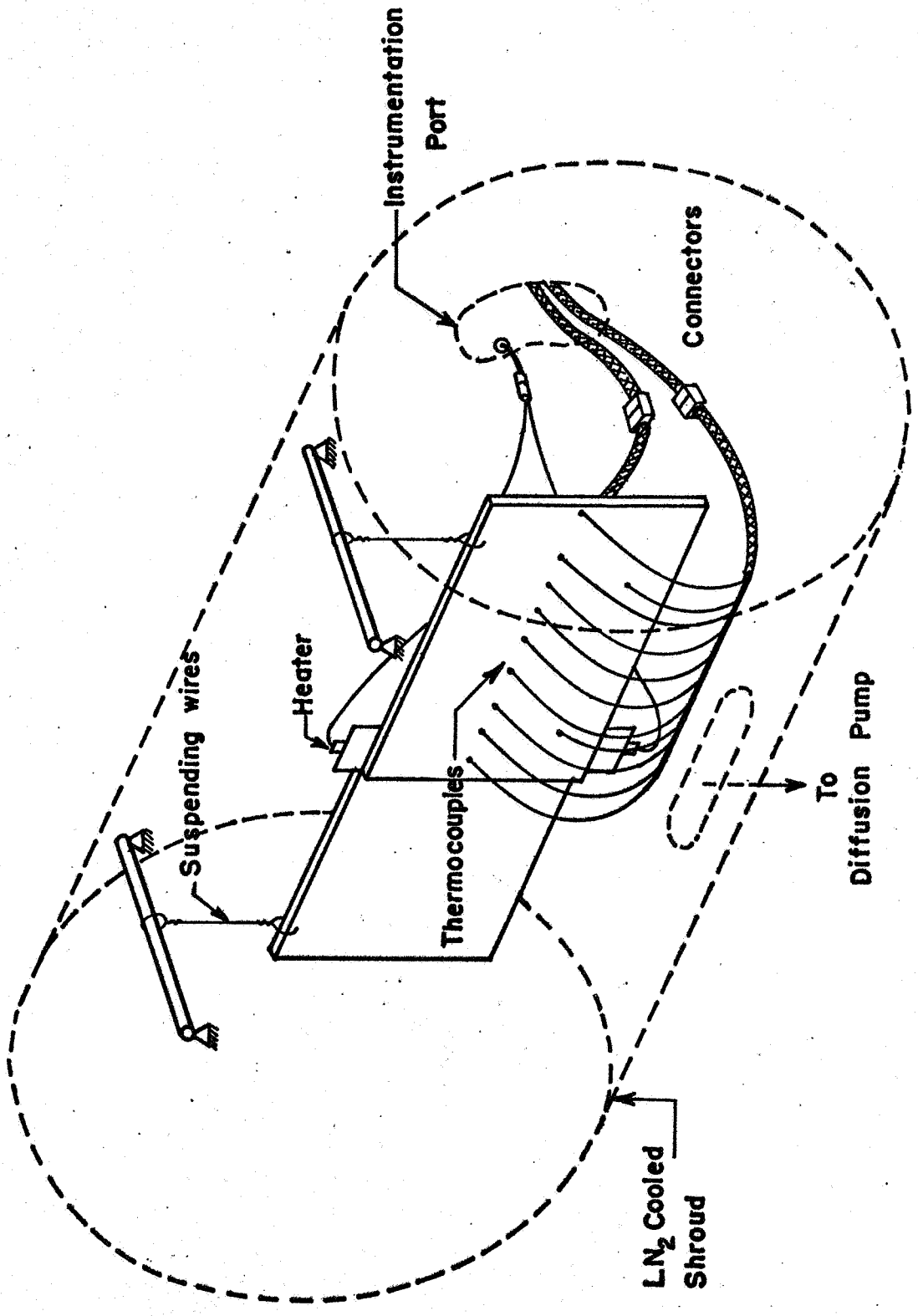

FIG. 6 ORIENTATION OF TEST OBJECT SUSPENDED IN CHAMBER

The transient response behavior of the system was studied by first operating the heater at a relatively low power level until a steady state temperature field was established.+ The power was then quickly raised and kept constant at a desired high level. All thermocouple outputs were continuously monitored and recorded during and after this disturbance. Fig. 7 shows schematically the input power variation and the accompanying temperature transients as may be exhibited by a typical thermocouple.

The second power level of the heater was established by the desired maximum temperature to which the test object was subject. In the present test series, it was in the neighborhood of 780°R (320°F). The first power level was somewhat arbitrary; it was chosen such that the average plate temperature was slightly above the room value. This temperature range roughly corresponds to that used in thermal conductivity measurements.

During the course of this investigation, it was discovered that the surface emittance of "Thermokote" aluminum 625 could not be reproduced within narrow limits (say less than 2 or 3%) in spite of all the known precautions taken, such as paint consistency, air pressure, spraying distance, number of spraying passes, drying time, etc. In addition, it was also found that the emittance changed when repeated tests were conducted on the same specimen. The cause of the latter change has not been definitely established but the contamination of the diffusion pump oil appeared to be a possibility. Every time when one opened the chamber door upon the completion of a test, one could unmistakably smell the oil. As a crude estimate, we could express the effect of emittance change on temperature variation by

$$\frac{\delta \epsilon}{\epsilon} \simeq -4 \frac{\delta T}{T} \quad \text{for } T^4 \gg T_{sh}^4 \tag{9}$$

if the heater power was kept constant (or, in the case of models, if the heater power was strictly proportional to the square of the geometric scale). Hence, a 4% change in emittance would result in a temperature change of

---

+ When the recorded temperature of any of the thermocouples indicated a change not more than 0.2°F per 30 minutes, steady state condition was assumed prevailing.

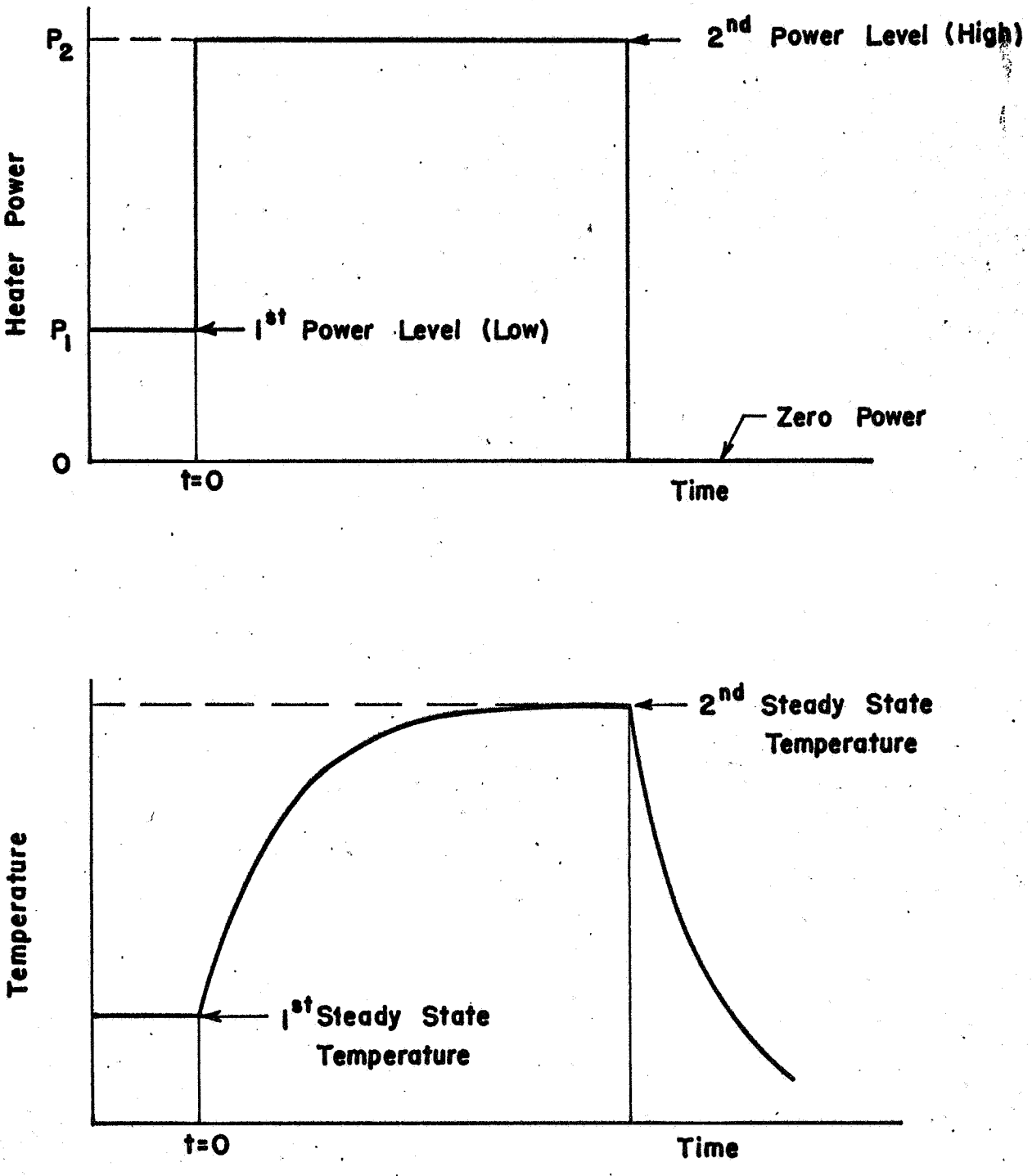

FIG. 7 HEATER POWER VARIATION AND ACCOMPANYING TEMPERATURE TRANSIENTS

7°R for T = 700°R. To overcome this difficulty, it was decided to evaluate the surface emittance in each test and correct for the change. This was done for the models as follows:

When the test object temperatures attained a steady state, all the thermocouple outputs and the heater power were measured and recorded. The average emittance was calculated from

$$\overline{\epsilon^*} = \frac{P^*}{\sigma \int_{A^*} [\,(T^*)^4 - \overline{T}_{sh}^4\,]\, dA^*} \qquad (10)$$

where P^* is the heater power, A^* is the total radiating area and $\overline{T}_{sh}$ is the average shroud temperature. A computer program was available for the evaluation. The two heater power levels shown in Fig. 7 were then adjusted to compensate for the emittance variation between the prototype and the models as according to:

$$\frac{P}{\epsilon} = \left(\frac{L}{L^*}\right)^2 \frac{P^*}{\overline{\epsilon}^*} \qquad (11)$$

During the heating up period from the first to the second steady state condition, some minor adjustment of the heater voltage was necessary to maintain a constant heater power due to changes of the heater resistance with temperature.

All test data were taken with chamber pressure maintained at approximately 5×10^{-7} torr and with about 3/4 of the shroud surface indicating a temperature of -310°F.

6. EXPERIMENTAL RESULTS--Configuration (a) only

6.1 Steady State Temperature Distributions

The average surface emittance as evaluated from (10) and the heater power normalized with respect to the average emittance for the prototype and the models are shown in Table III. As pointed out in the previous section, for reasons not clear to us at the present time, the emittance

TABLE III. MEASURED AVERAGE SURFACE EMITTANCE AND HEATER POWER FOR THE FIRST AND SECOND STEADY STATE

		Prototype	$\frac{1}{2}$-Scale Model	$\frac{1}{4}$-Scale Model
Average Emittance	1st Steady State	0.303	0.281	0.305
	2nd Steady State	0.320	0.281	0.310
Heater Power Btu/hr	P_1	286.3	65.8	18.0
	P_2	810.0	175.1	48.5
$\frac{P_1}{\epsilon}$		944.9	234.2	59.02
$\frac{P_2}{\epsilon}$		2531	623.1	156.5
$\frac{P_1^*}{\epsilon^*} \times \left(\frac{L}{L^*}\right)^2$		944.9	936.8	944.3
$\frac{P_2^*}{\epsilon^*} \times \left(\frac{L}{L^*}\right)^2$		2531	2492	2504

of surfaces painted with "Thermokote" aluminum 625 was difficult to reproduce within close limits. When the normalized heater power of the model is multiplied by the square of the geometric scale ratio $\left(\frac{L}{L^*}\right)^2$, the result should, in theory, be identical to the $\frac{P}{\epsilon}$ of the prototype. The minor discrepancies shown in Table III are due to differences in the steady state temperatures of the prototype and the model from which the emittances are evaluated.

The measured steady state temperature distributions for both materials are shown in Figs. 8 - 1 and 8 - 2. In order to render the data from the prototype and the models directly comparable, the abscissa is plotted in a dimensionless length coordinate η which is the distance measured in units of plate length along the center line and from the edge of the plate adjacent to the heater. Clearly, any fixed value of η would correspond to homologous locations in the prototype and the models.

An inspection of both figures indicates that the overall prediction of prototype temperature distributions at both low and high heater power by modeling technique introduced in this investigation can be described as satisfactory. The agreement is generally better at the low heater power. Large errors up to 16°R appeared in the region close to the heater at the high power level. Undoubtedly, the heat flow in such a region would have a significant component normal to the plate surface. In Fig. 8 - 2, the temperature profile plotted from the $\frac{1}{2}$-scale model data crosses with the prototype profile. It is thought that the relatively large discrepancies in surface emittance of the prototype and of the $\frac{1}{2}$-scale model might be the cause, but no conclusive evidence can be given. At the time when this report is in preparation, the incomplete test data for Configuration (b) indicate considerable better agreement between prototype steady temperature profiles and those predicted by the models. These results will be reported in the future.

A somewhat unexpected finding is that the predictions from the $\frac{1}{4}$-scale model are consistently better. One reason is that the measured average emittance of the $\frac{1}{4}$-scale model is more close to that of the prototype. Another is that the experience gained in the installation of thermocouples, establish-

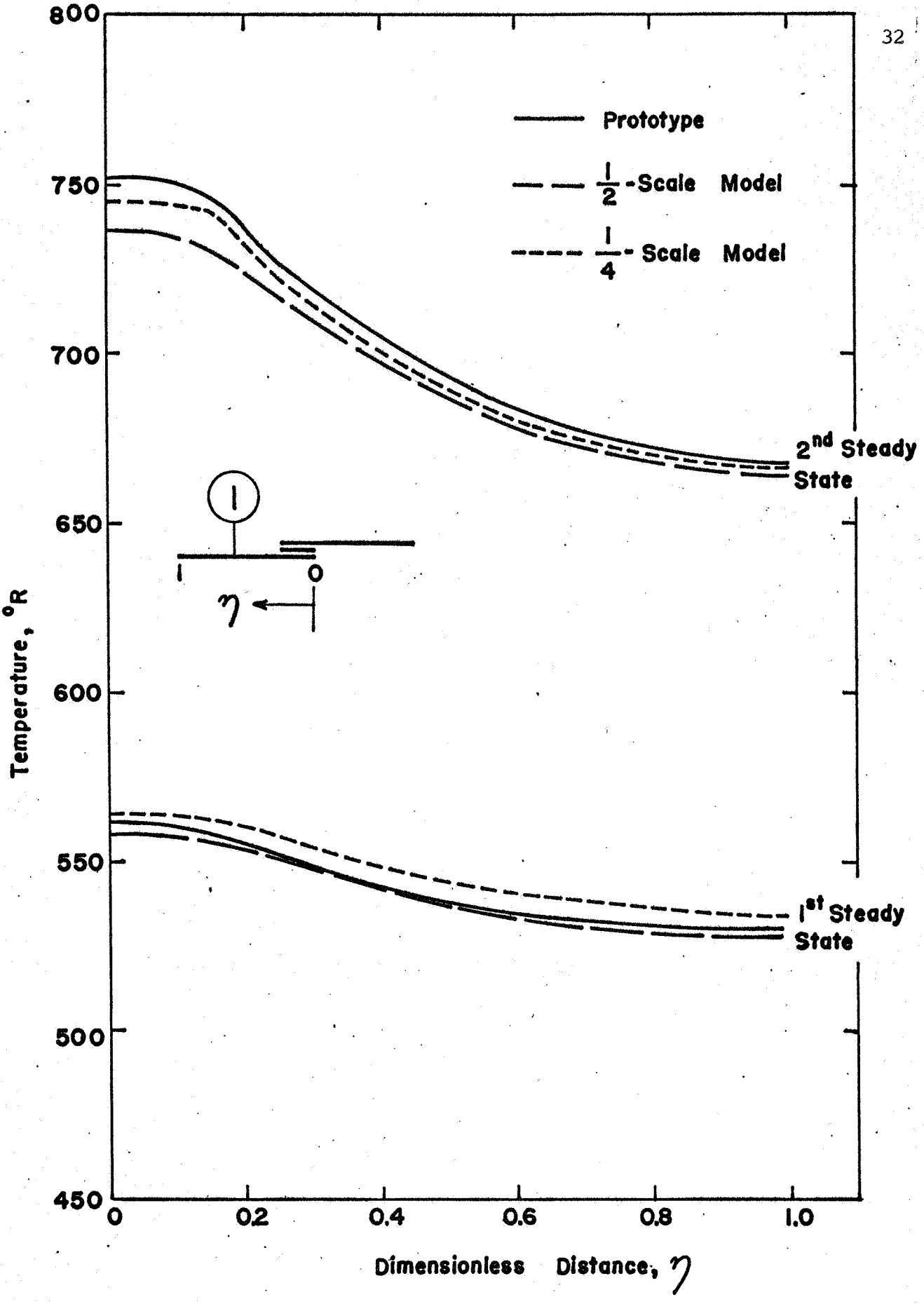

FIG. 8-1 STEADY STATE TEMPERATURE DISTRIBUTION-CONFIGURATION (a), MATERIAL (1)

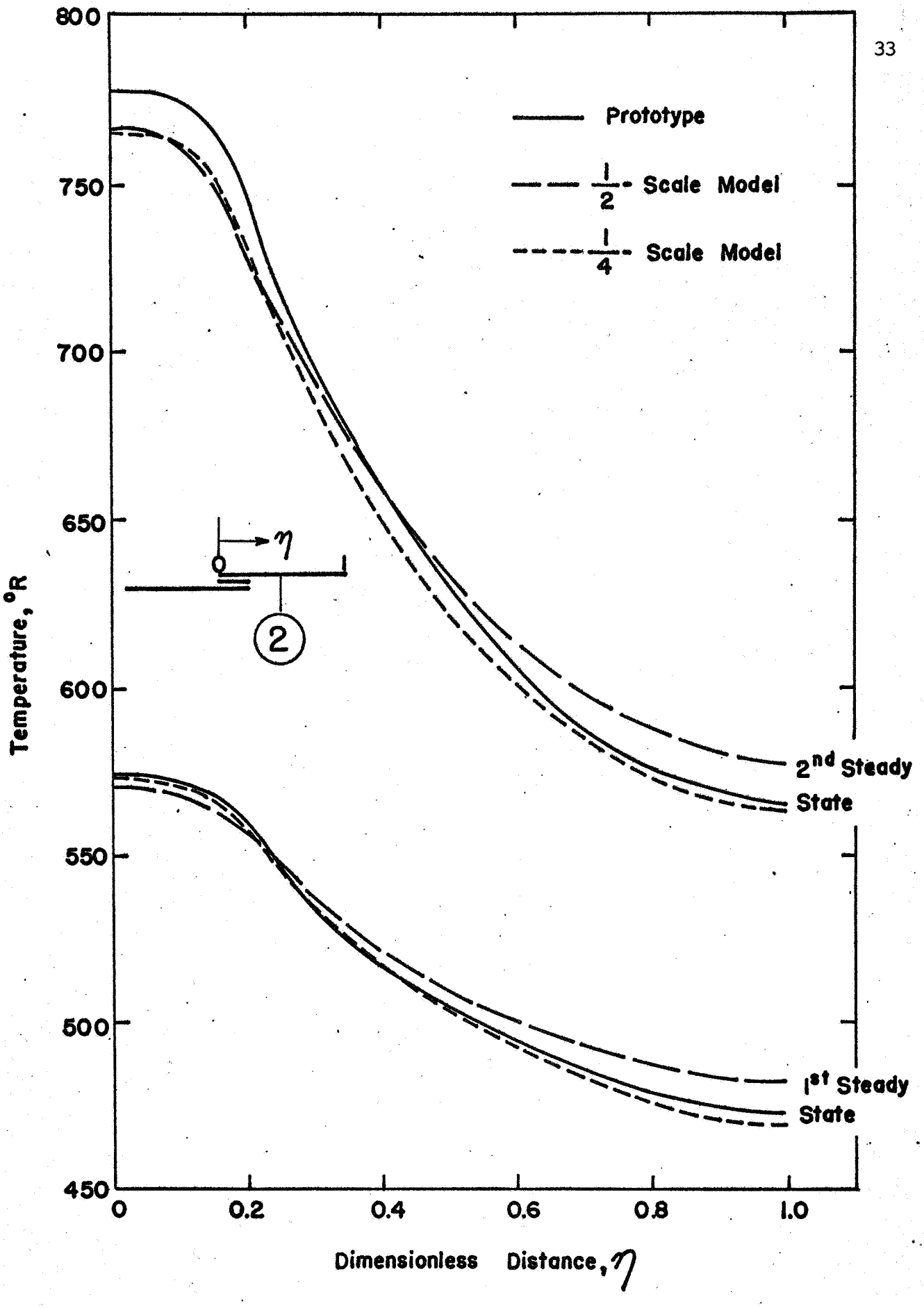

FIG. 8-2 STEADY STATE TEMPERATURE DISTRIBUTION - CONFIGURATION (a), MATERIAL (2)

ment of chamber conditions, data recording procedure, etc., during tests performed on the prototype and the $\frac{1}{2}$-scale model has been of considerable value in our continuing effort to reduce experimental errors. Also, the error involved in the thickness measurement of the electrodeposited copper layer is probably quite large. Since the .00279 inch copper plating on the nickel-silver surface of the $\frac{1}{2}$-scale model has a significant contribution to the overall effective conductance, errors due to such source will certainly be reflected in the recorded temperatures.

6.2 Transient Results

Figs. 9 - 1 through 9 - 3 exhibit the heating and cooling curves at several indicated locations in material (1) for the prototype and the models. Similar curves for material (2) are shown in Figs. 10 - 1 through 10 - 3. In all figures, the abscissa is the prototype time which, in the case of models, is the actual time divided by the appropriate time scale listed in Table II. The upward arrow ↑ designates the instant when the heater power was rapidly increased from P_1 to P_2. Prior to this change, the system was at the first steady state condition. The downward arrow ↓ designates the instant when the heater power was completely turned off.

It is seen that, using the modeling technique introduced in this investigation, the transient response behavior of the prototype could be predicted with an accuracy comparable to the steady state temperatures. Largest errors generally occurred at those locations where the heat flow had a significant component normal to the plate surface (thermocouple 9_1 and 9_2), particularly when the system approached the second steady condition. Heating and cooling curves for other thermocouple locations shown in Fig. 3 were all recorded but not presented in the interest of saving space; they exhibit errors less than those shown in Figs. 9 - 1 and 10 - 1. In no instance, the predicted temperatures by the $\frac{1}{2}$-scale model were more than 16°R in error which was the maximum observed among the steady temperatures. If one takes into account the readings of all thermocouples for all times, it is estimated that the average error would be less than half the maximum. The predictions from the $\frac{1}{4}$-scale model are decidedly better. The maximum error was about 11°R with an average probably around 5°R.

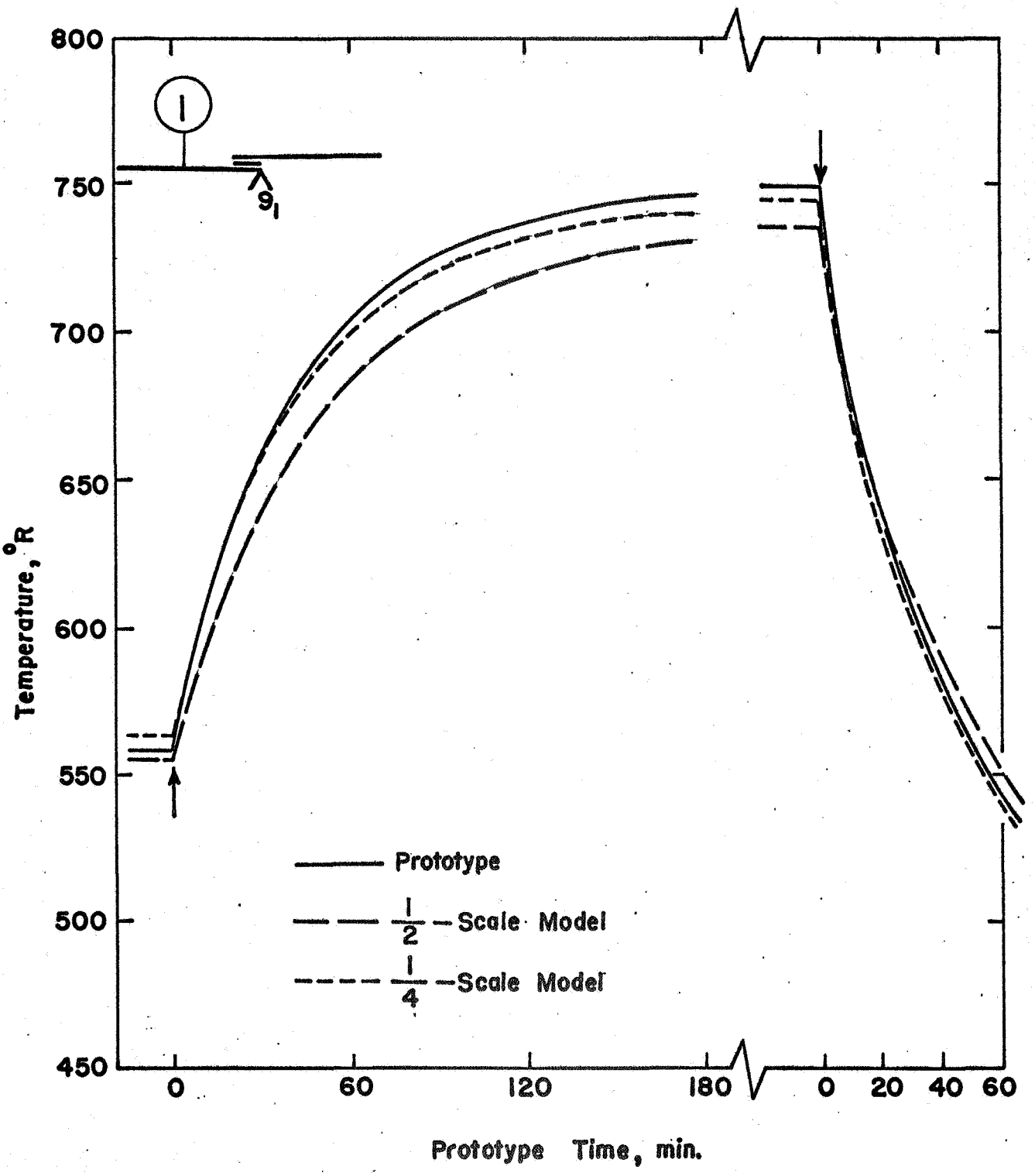

FIG. 9-1 HEATING AND COOLING TRANSIENTS AT LOCATION 9_1

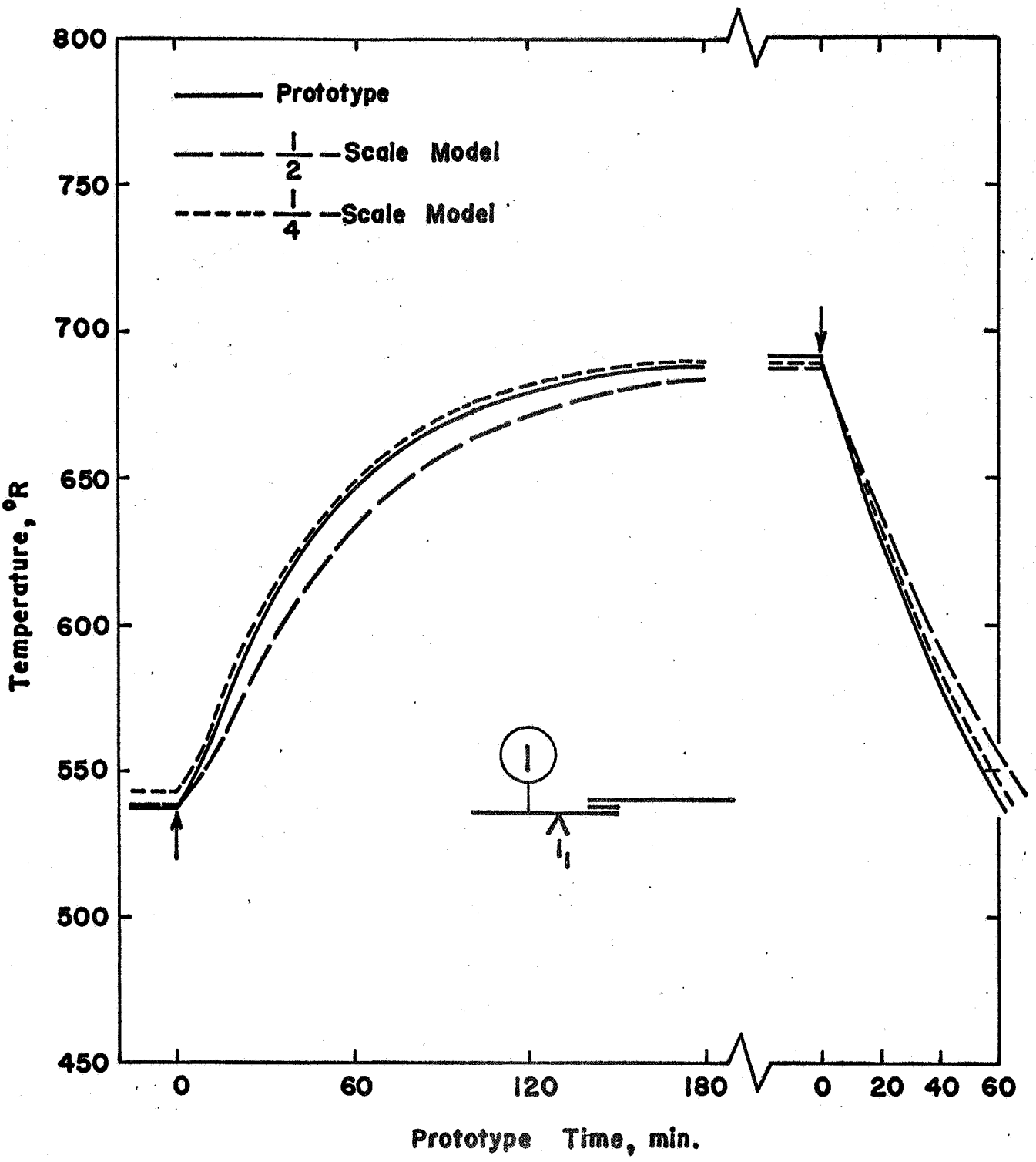

FIG. 9-2 HEATING AND COOLING TRANSIENTS AT LOCATION l_1

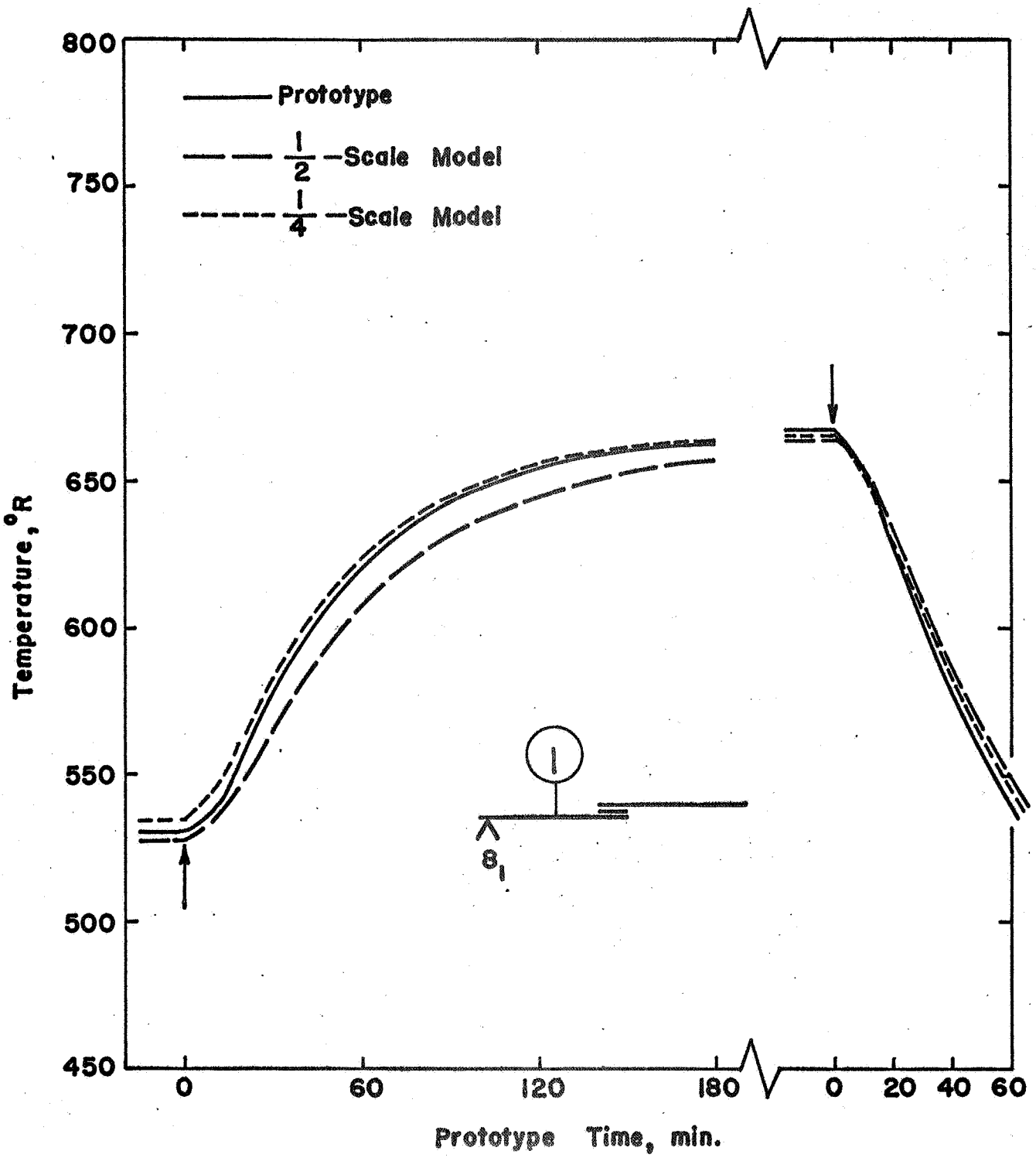

FIG. 9-3 HEATING AND COOLING TRANSIENTS AT LOCATION θ_1

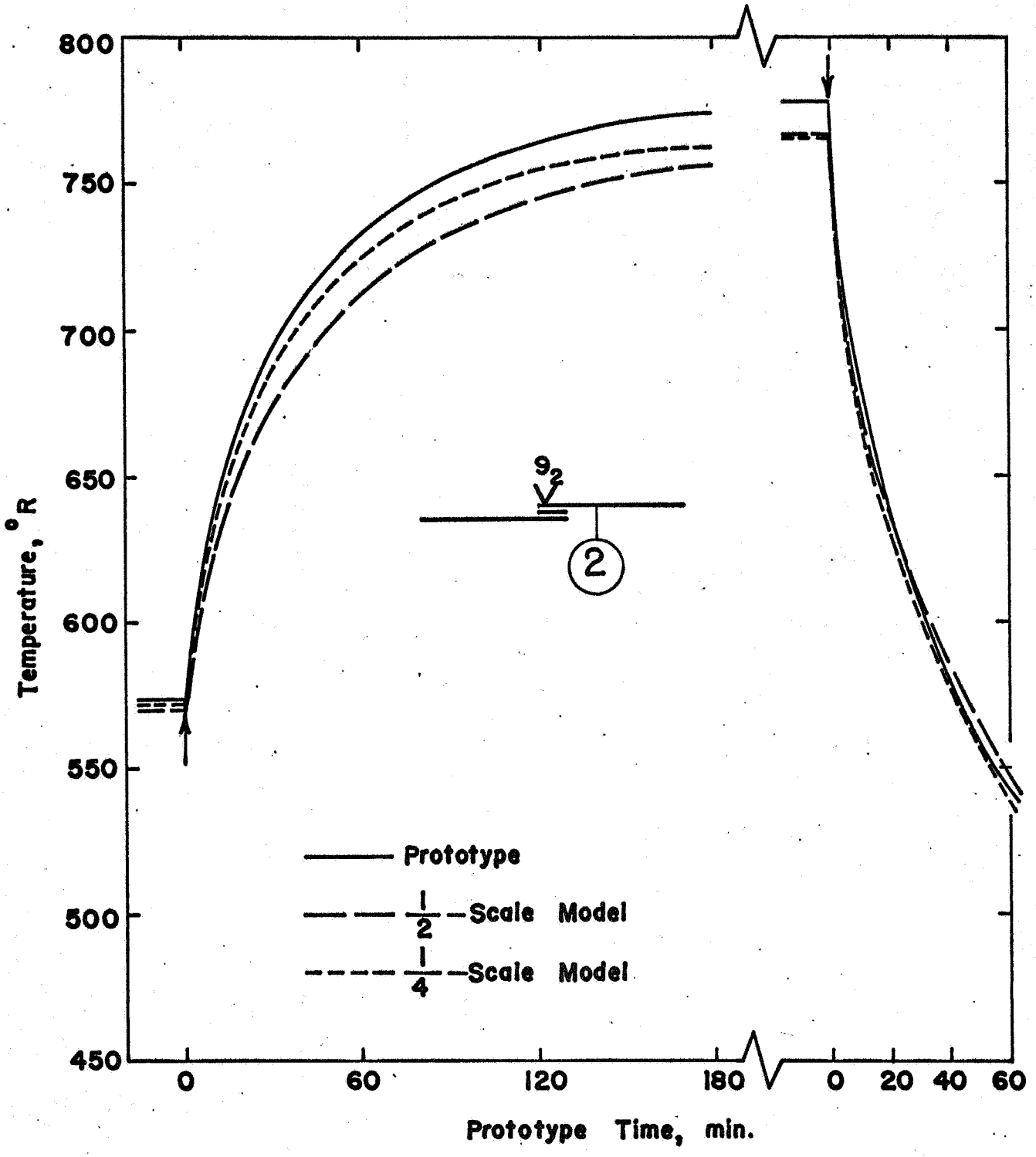

FIG. 10-1 HEATING AND COOLING TRANSIENTS AT LOCATION θ_2

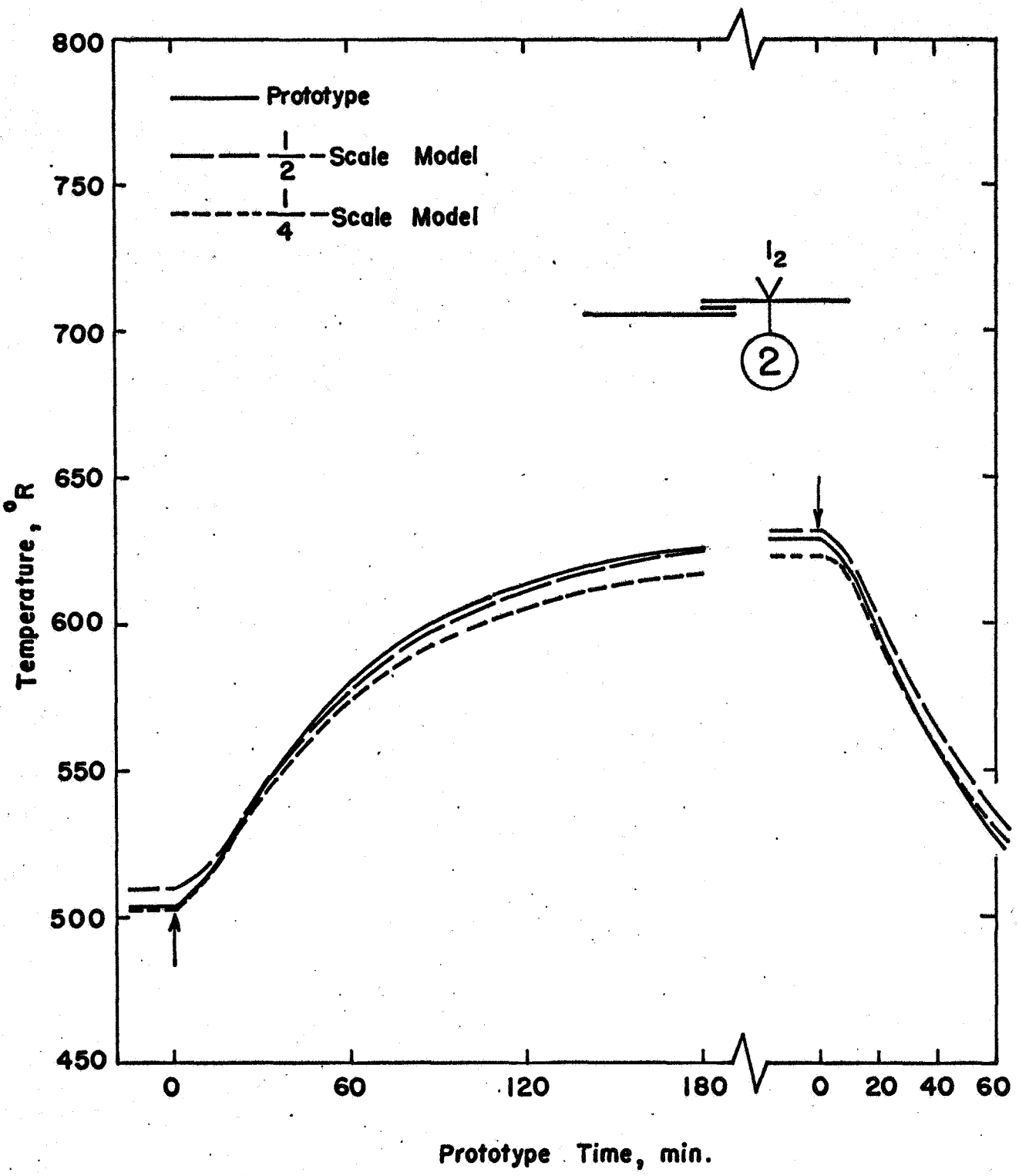

FIG. 10-2 HEATING AND COOLING TRANSIENTS AT LOCATION l_2

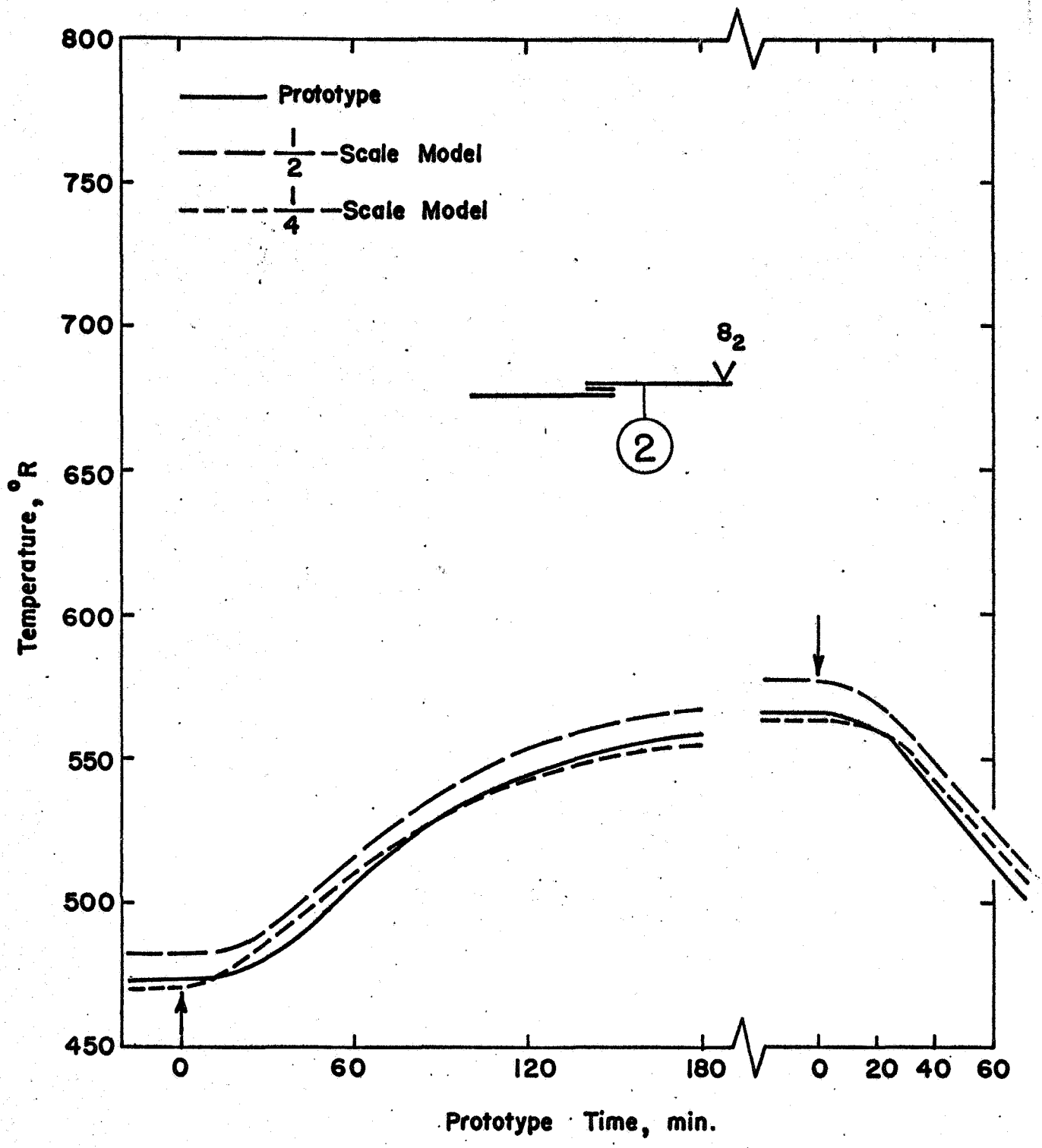

FIG. 10-3 HEATING AND COOLING TRANSIENTS AT LOCATION θ_2

When the heater power was switched off from the second steady state, the relatively high temperature plate surfaces were quickly losing heat to the surrounding blackened cold shroud surface as manifested by the steep slopes of the cooling curves shown in Figs. 9 and 10. The heat transfer process was dominated by surface radiation with internal conduction playing a secondary role. Under such conditions, the most significant similarity requirement pertains to the model time scale ratio, i.e.

$$\frac{t^*}{t} = \frac{\overline{C^* d^*}}{\overline{C\ d}} \quad \frac{\epsilon}{\epsilon^*} \tag{12}$$

which should be a constant for both materials. Criterion (12) differs from (2) in that it contains the emittance ratio to account for the observed variation in ϵ of the prototype surfaces and those of the models. The cause of the discrepancies which existed among the cooling curves as displayed in Figs. 9 and 10 should be sought in terms of the departure from the exact satisfaction of (12).

On the other hand, as the system gradually approaches steadiness, the time rate of internal energy change would become less and less significant in the overall energy balance. The major similarity requirement then becomes

$$\left(\frac{L^*}{L}\right)^2 = \frac{\overline{k^* d^*}}{\overline{k\ d}} \quad \frac{\epsilon}{\epsilon^*} \tag{13}$$

which is also a constant. The foregoing observation suggests the possibility of the separation of error sources and, thus, may lead to the development of a correction procedure for imperfect modeling.

7. TENTATIVE CONCLUSIONS AND RECOMMENDATIONS

In view of the fact that results for system configurations (b) and (c) are not yet available, the several conclusions given below can only be regarded as tentative.

(1) The technique of artificially modifying the effective conductivity of metal plates or sheets by electrodeposition in order to satisfy transient

modeling requirements of systems involving more than one material seems quite feasible. More work need be done so that the uniformity and thickness of the plating could be controlled with high precision.

(2) The emittance of the thermal paint, "Thermokote" aluminum 625, seems difficult to reproduce within close limits in spite of all the precautions taken in paint preparation, in controlling the spraying and drying procedure, etc. For simple structures, like those tested in this investigation, small discrepancies in surface emittance could be accounted for by a procedure described in Section 5 of this report. In testing models of actual spacecraft, every effort need be made to ensure identical surface properties of corresponding components, particularly for those surfaces which control the spacecraft thermal behavior.

(3) Using the modeling technique developed in this investigation, the general prediction of prototype temperatures, both steady and transient, is satisfactory. Predictions by the $\frac{1}{4}$-scale model are no less accurate than those by the $\frac{1}{2}$-scale model and transient errors are no more than steady state errors. In regions where the heat flow has a significant component normal to the surface, large errors are likely to exist.

(4) Proper installation procedure for thermocouples should be strictly observed. Checking their responses prior to actual testing almost seems mandatory.

(5) While the results of the experiments conducted so far lend support to the theoretical requirements and the suggested design procedure for the transient thermal modeling of systems involving radiation and conduction heat transfer, they also demonstrate that "exact" modeling is impractical to attain. This is especially true when the complicated, real spacecrafts have to be modeled. Hence, to develop an understanding of the nature of errors, to introduce a procedure of effecting simplifications and to devise a method of applying corrections for imperfect modeling should receive top consideration.

8. REFERENCES

[1] J. M. F. Vickers, "Thermal Scale Modeling," Advanced Heat Transfer Lectures, University of Illinois, Urbana, April, 1967, p. 663.

[2] J. M. F. Vickers, "Thermal Scale Modeling," Astronautics & Aeronautics, V. 3, No. 5, 1965, p. 34.

[3] B. P. Jones, "Theory of Thermal Similitude with Applications to Spacecraft--A Survey," Astronautica Acta, V. 12, No. 4, 1966, p. 258.

[4] F. Gabron, "Spacecraft Thermal Scale Modeling," Short Course Lecture Notes, University of California, Los Angeles, April, 1967.

[5] D. L. Adkins, "Scaling of Transient Temperature Distributions of Simple Bodies in a Space Chamber," Paper No. 65-660, AIAA Thermophysics Specialist Conference, Monterey, California, September, 1965.

[6] B. P. Jones and J. K. Harrison, "A Set of Experiments in Thermal Similitude," NASA TMX-53346, October, 1965.

[7] R. E. Rolling, "Thermal Scale Modeling in a Simulated Space Environment," Lockheed Palo Alto Research Laboratory Report, June, 1966. Major contents of this report also appear in two papers by the same author: "Results of Transient Thermal Modeling in a Simulated Space Environment," Paper No. 65-659, AIAA Thermophysics Specialist Conference, Monterey, California, September, 1965, and "Thermal Modeling of a Truncated Cone in a Simulated Space Environment," AIAA/IES/ASTM Space Simulation Conference, Houston, Texas, September, 1966.

[8] P. L. Miller and J. A. Wiebelt, "Thermal Modeling in a Simulated Space Environment," Paper No. 67-305, AIAA Thermophysics Specialist Conference, New Orleans, Louisiana, April, 1967.

[9] N. R. Folkman, E. L. Baldwin and J. B. Wainwright, "Tests on a Thermally Scaled Model Space Station in a Simulated Solar Environment," Paper No. 65-658, AIAA Thermophysics Specialist Conference, September, 1965.

[10] R. L. Young and R. V. Shanklin, III, "Thermal Similarity Study of a Typical Space Vehicle Element," Journal of Spacecraft and Rockets, V. 3, No. 12, 1966.

[11] B. T. Chao and G. L. Wedekind, "Similarity Criteria for Thermal Modeling of Spacecraft," Journal of Spacecraft and Rockets, V. 2, No. 2, 1965, p. 146.

APPENDIX 1

THERMAL CONDUCTIVITY MEASUREMENT

As is obvious from the modeling criteria given in Section 3.2 of this report, information on both the thermal conductivity and heat capacity of the materials used in the experiments is essential. Unfortunately, such information of sufficient reliability is not readily available. While Refs. [1], [2], [3], [4] and [5] of this Appendix gave extensive tabulation of both k and C_p for pure metals, conductivity data of metal alloys are far from being adequate. Discrepancies among different sources are not uncommon. As an illustration, let us take aluminum bronze D (copper alloy No. 614) which is one of the two materials selected for the construction of the prototype. Its nominal composition and commercial limits are shown below.

	Nominal	Commercial Limits	
		Maximum	Minimum
Copper	91	-	-
Aluminum	7	6.0	8.0
Iron	2	1.5	3.5
Manganese	-	-	1.0
Cu + Aℓ + Fe + Mn : 99.5% minimum			

Reference [3] reported its conductivity to be 44 Btu/hr - ft - °F at 68°F while a value of 39 was listed in [4] for the same temperature. Reference [5] reported an average value of 40.8 Btu/hr - ft - °F for temperatures ranging from 32°F to 212°F.

A commercial grade pure nickel with nominal composition of 99.4% Ni and a maximum of 0.02% C was used in the $\frac{1}{4}$-scale model. It is designated as

nickel L. Its conductivity data for the temperature range of 591°R to 850°R were given in [1] but the scatter is unusually widespread. The following was taken from a plot shown on p. 449 of Volume I of that reference.

Temperature: °R	590	620-625	810-825	850
k (in Btu/hr - ft - °R)	48.8	47.3, 39.8	60, 52.7, 44.8	34.7

Clearly such information is of doubtful value to the present investigation. Reference [5] reported an average value of 35 Btu/hr - ft - °R for the temperature range of 492°R to 672°R.

It is well known that the thermal conductivity of pure metals is, in general, very sensitive to impurities and this may very well be the reason for the large scatter of data which one finds for commercially pure metals. The thermal conductivity of metal alloys depends not only on their chemical composition but also on their metallographic structure. The latter depends to a great extent, on the history of their chemical and thermal treatment. Unfortunately, such information is generally not accurately prescribed for commercially available stocks. Nor is their chemical composition held within close limits. It is for these reasons that a decision was made to measure the conductivity of all materials used in the modeling experiments in our own laboratory. On the other hand the heat capacities of metal elements are known and those for alloys can be calculated from the Neumann and Kopp's rule within an accuracy of a few percent. Thus, because of the lack of adequate facility and of time shortage, they are not measured.

A1.1 Experimental Methods

Experimental methods for measuring the thermal conductivity of materials, using either transient or steady state technique, have been extensively described in the literature. The choice among them would depend on (a) the material shape (e.g. powders vs. bulk solid), (b) whether the material is a good or poor conductor, (c) the desired accuracy of the data, and (d) time

and financial resources available. After weighing the several factors involved, it was decided to use the steady state method. The test specimens were in the form of rods of constant cross section and were fabricated from the same metal sheets or plates used in the modeling experiments. The exposed surfaces of the test specimen were covered with low emittance aluminum foil tape and the tests were conducted in a vacuum chamber, the walls of which were lined with aluminum paper.

The physical basis of the experiment is the one-dimensional Fourier conduction equation which states that the rate of heat flow Q through any cross section of the rod is equal to the negative of the product of the local thermal conductivity k, its sectional area A, and the local temperature gradient $\frac{dT}{dx}$. Thus,

$$Q = -kA\frac{dT}{dx} . \qquad (A1.1)$$

Since our objective is to obtain conductivity data with an accuracy of approximately 2%, the success depends to a very great extent on our ability to obtain reliable temperature and heat flow measurement. A brief description of the experimental system will first be given in the next section. This will be followed by a discussion of the procedure used in evaluating the heat loss and, thence, the determination of the heat flux in the test specimen. An error analysis is also presented.

A1.1.1 The Experimental Apparatus and Test Specimen Preparation

A test facility originally built for studying thermal contact resistance is available in the Heat Transfer Laboratory. It was conveniently adapted for the present purpose after some minor modifications. The facility consists of a vacuum chamber, a power supply and the associated instrumentation. A cartridge heating element installed inside an oxygen-free high conductivity copper block supplies heat to one end of the test specimen. A similar copper block with cooling water passage was provided at the other end to remove the heat. The heating source, test specimen, and the water cooled sink was assembled into a vertical column and loaded axially by means of

two hardened steel balls in contact with Mycalex insulator to minimize heat leak. Fig. A1-1 shows schematically the arrangement of the test column when installed in place in the vacuum chamber.

For reasons already explained in the introductory paragraphs of this Appendix, the test specimens were fabricated from the same metal sheets or plates used in the model experimentation. They were cemented together by an epoxy adhesive which was cured under pressure. The cemented sheets were then machined to produce a specimen of 3/4 or 1/2 inch square section (specimens of rectangular cross section, 1/2 inch x 3/4 inch, had also been used). Examination of the completed specimen under the microscope revealed that the layer of adhesive was reasonably uniform and had a thickness of approximately 0.003 to 0.004 inch. The conductivity of the epoxy cement is not known but was estimated by the vendor to be not greater than 0.2 Btu/hr - ft - °R. For all test specimens, its conductance relative to that of the metal plates is completely negligible (<0.1%). A copper cap was soldered to each end of the test specimen using Eccobond 56C solder which is a high conductance adhesive. The copper caps served the useful purpose of producing a nearly isothermal surface at each end of the specimen.

Nine 30 AWG copper-constantan thermocouples, spaced $\frac{1}{2}$ inch apart, were mounted along the length of the test specimen. Special precision wires were employed and calibrated to within 0.1 F. These thermocouples were installed in 0.031 inch holes drilled slightly beyond the half-depth of the specimen. The center to center distance among the holes were determined from a microscope equipped with a filar measuring head. It was estimated that the spacing among the thermocouple junctions was obtained within an accuracy of 0.005 inch.

A photograph of typical specimens with thermocouples and Wenchester quick change connectors is shown in Fig. A1-2. The larger specimen at the left, shown with the copper caps detached, has a 3/4 inch square section. It consists of eight thin plates of nickel silver cemented together. The specimen at the right, fabricated of 5086 aluminum, is shown with the copper caps soldered to position. The aluminum foil tape which covered its surface could also be seen.

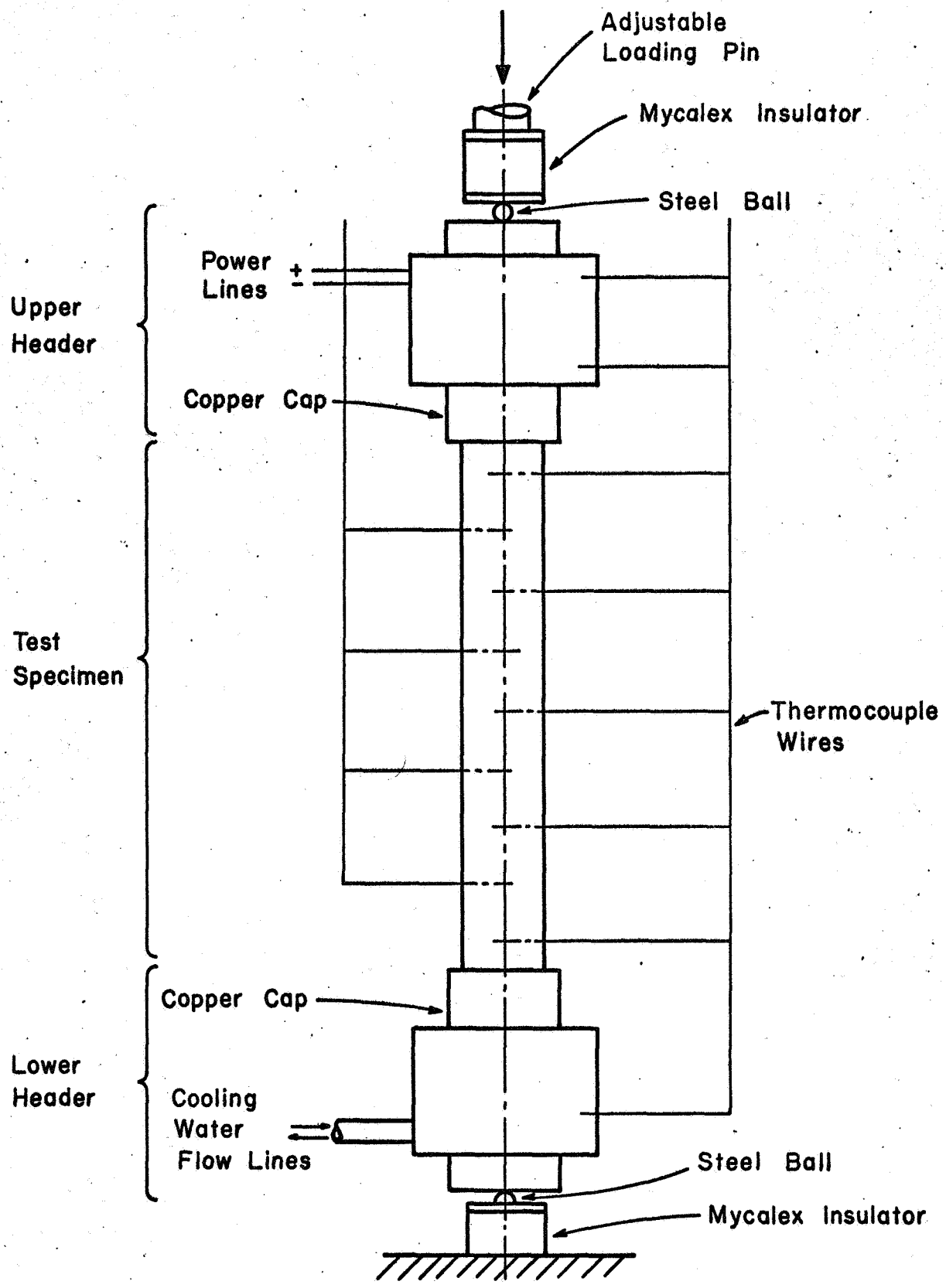

FIG. A.1-1. TEST COLUMN ASSEMBLY FOR THERMAL CONDUCTIVITY MEASUREMENT.

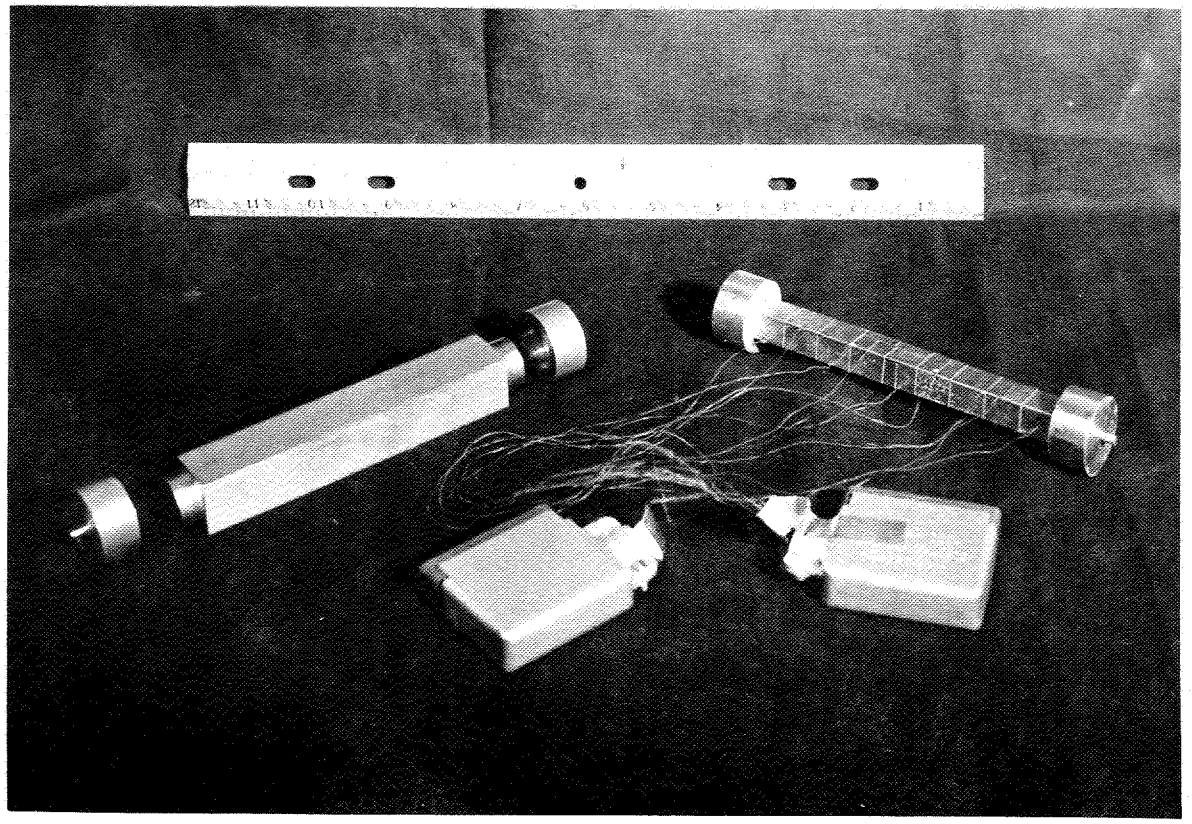

FIG. AI-2 TEST SPECIMENS FOR CONDUCTIVITY MEASUREMENT

The chamber was evacuated by a 1405 H Welch mechanical pump in series with a Consolidated Vacuum Corporation VMF-20 diffusion pump. A pressure of about 2×10^{-5} mm Hg was maintained throughout the tests. It has been established in [6] that at such pressure level the convective losses are negligible.

The interior surface of the chamber, the cooling water tubes, the thermocouple connectors and all the other components which could see the test column were covered with aluminum wrapping paper. Two thermocouples, one each attached near the upper lower end of the cylindral surface of the upper copper header, monitored temperatures for heat loss evaluation. The chamber wall temperature was also measured.

A1.1.2 Input Power and Temperature Measurement

The electrical energy supplied to the cartridge heater was from an adjustable d.c. power supply. Voltage and current measurements were made respectively with a multi-range Weston voltmeter and a Hallmark precision 0.35% instrument.

All thermocouples were provided with individual cold junctions immersed in an ice bath. Their thermal emf's were measured with a Leeds and Northrup 8686 potentiometer. Within the temperature range of interest, the error was estimated to be about three microvolts which correspond to 0.15°F. The absolute error in measured temperatures was, of course, much larger. However, insofar as the conductivity determination is concerned, only the relative error is of relevance. The latter has been estimated to be not more than 0.2°F.

A 24-point L & N selector switch made convenient successive reading of the thermocouples. A multi-range, single point millivolt recorder was also connected in the measuring circuit. It served the useful purpose of visually indicating the attainment of steady heat flow condition in the test specimen and also of double checking the temperature readings.

A1.1.3 Heat Loss Determination and the Conductivity Tests

To evaluate k from Eq. (A1.1), it is necessary to determine the local

heat flow rate Q in the test specimen in addition to its temperature distribution. Referring to Fig. (A1.3), it is seen that a portion of the heat generated by the heater is lost to the surroundings before it enters the test specimen. Denoting the total rate of heat generation by Q_t, the heat which enters the test specimen per unit time by Q_e, that which is lost at the upper header by $Q_{\ell(h)}$ and that which is lost from the portion of the specimen surface between x = 0 and x = x by $Q_{\ell(x)}$, we may write for steady state condition,

$$Q_e = Q_t - Q_{\ell(h)} \qquad \text{(A1.2a)}$$

and

$$Q = Q_e - Q_{\ell(x)} \cdot \qquad \text{(A1.2b)}$$

In the present series of experiments, $Q_{\ell(h)}$ ranges from approximately 10 to 30% of Q_t, depending on the temperature of the upper header, the chamber wall temperature, the geometry and surface properties of the radiation shield interposing between the header and the chamber wall and the relative magnitude of Q_e and Q_t which, in turn, depends on the conductance of the test specimen. The last effect was small but was definitely observed during the course of the investigation. This was due to the fact that the temperature of the upper header was not uniform and its heat loss would be influenced by its surface temperature distribution. For this reason, $Q_{\ell(h)}$ was separately determined for each test specimen. It was evaluated immediately following the regular conductivity test run <u>without disturbing the test column assembly</u>.

The heat loss from the test specimen surface, $Q_{\ell(x)}$, was relatively small but not completely negligible, particularly when the specimen was of low conductivity. It was calculated from the measured specimen temperature distribution and the previously determined surface emittance of the aluminum foil tape. In what follows, we shall describe the procedures used for the determination of $Q_{\ell(h)}$ and $Q_{\ell(x)}$.

As had already been emphasized, the determination of $Q_{\ell(h)}$ was an integral part of the test routine. The heat loss evaluation test differed from the conductivity test only in that the cooling water through the lower

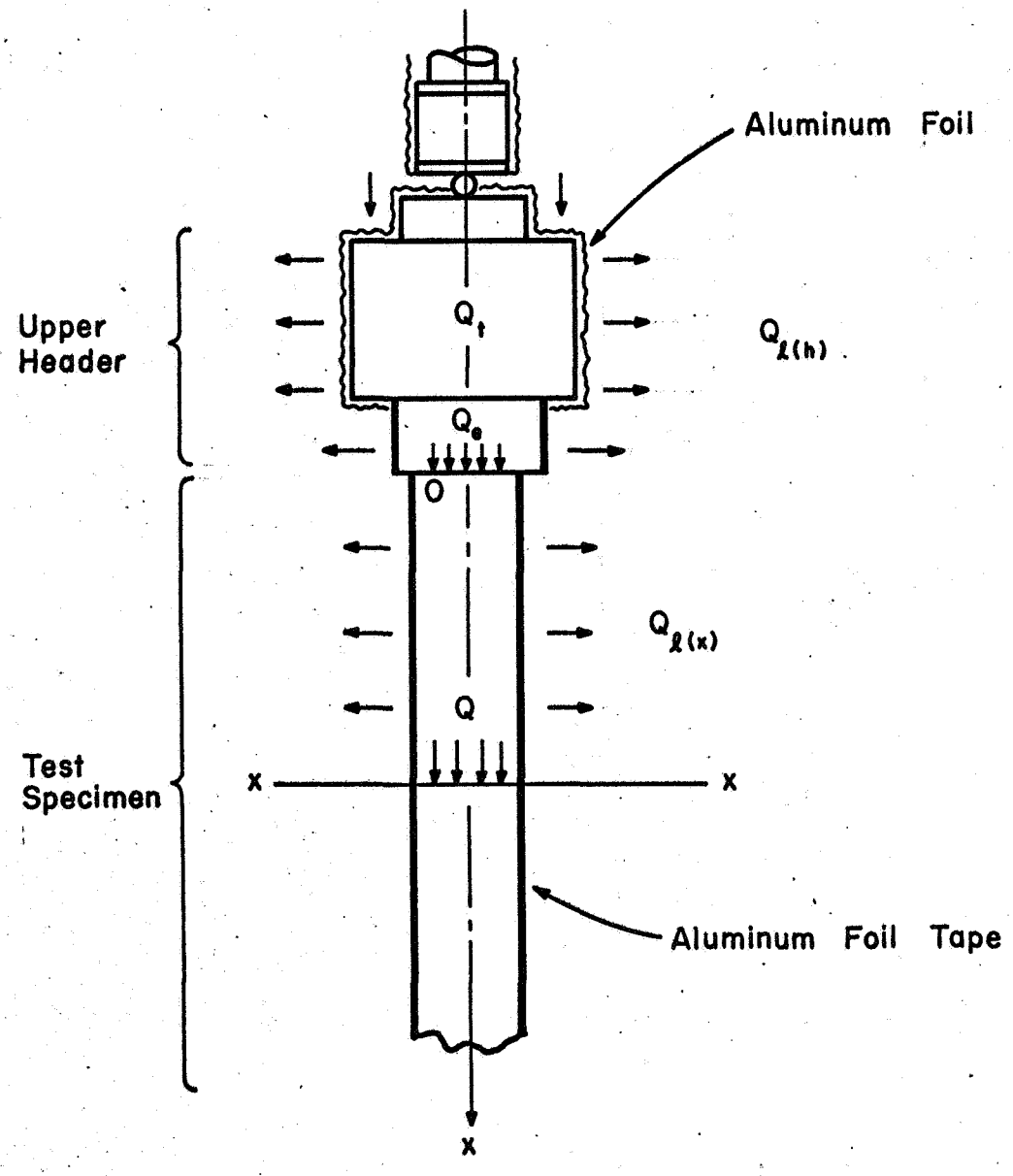

FIG. A1-3. TEST COLUMN HEAT LOSSES.

header was disconnected, thus reducing the heat flow through the specimen to a minimum. The power level was so adjusted that the average temperature of the upper copper header fell within the temperature range chosen for the conductivity test runs. The tests were repeated for different input power levels to cover the entire temperature range. During each test, the average surface temperature of the upper header $\bar{T}_h$ (taken as the arithmetic mean of the two surface thermocouple readings) and the chamber wall temperature T_w were measured and recorded. The latter differed only slightly from the room temperature and varied from 80°F to 90°F.

The temperature data read from the nine thermocouples installed along the length of the test specimen were fitted with a second degree polynomial using the least square procedure. A simple computer program was written for this purpose. In all tests, data were recorded after the attainment of steady state condition which was arbitrary taken as that when the thermocouple readings showed a variation of less than 0.1°F over a period of one hour.

Denoting all qualities associated with a heat loss test by an asterisk, we could write

$$Q^*_{\ell(h)} = Q^*_t - Ak^* \left|\frac{dT^*}{dx}\right|_{x=o} \qquad (A1.3)^{\dagger}$$

for any given temperature difference $\Delta T(\equiv \bar{T}_h - T_w)$ under consideration. In Eq. (A1.3), k^* is the conductivity of the specimen at temperature T^* $(x = 0)$, the latter was evaluated by setting $x = 0$ in the computer fitted second degree polynomial for the measured temperature distribution. However, k^* is not a priori known but could be determined by a simple iterative procedure using information deduced from the conductivity test as explained below.

The conductivity test runs and their data acquisition and processing procedure were essentially identical to those for the heat loss tests. For

---

†The two vertical bars denote absolute value.

the same ΔT, we may write

$$Ak \left|\frac{dT}{dx}\right|_{x=0} = Q_t - Q^*_{\ell(h)} \,. \qquad \text{(A1.4)}\dagger$$

The assumption made here is that the upper header heat loss depends only on ΔT. This is not strictly true because the surface temperature distribution of the upper header during the conductivity test proper deviates somewhat from that during the heat loss test even though its average temperature is the same. However, the error due to this source has been found to be less than 0.5% in all cases.

An iterative procedure using alternately Eq. (A1.3) and Eq. (A1.4) was employed to determine k^*, $Q^*_{\ell(h)}$, and k. We began by assuming a suitable k^* (published information, if available, for similar material could very well serve this purpose) and computed $Q^*_{\ell(h)}$ in accordance with Eq. (A1.3). The temperature gradient $(\frac{dT^*}{dx})_{x=o}$ was evaluated by finding the slope at x = o of the second degree polynomial for the temperature distribution. This approximate value of $Q^*_{\ell(h)}$ was then inserted in Eq. (A1.4) to determine k which now served as an improved estimate for k^*. The process was repeated until k^* and k agreed within 1%. This iterative procedure was found to be rapidly convergent; only two or three cycles of computation were required. If one begins by taking $Q^*_{\ell(h)}$ to be equal to Q_t^*, the process would still converge but more iterations are required to obtain results of comparable precision.

The preceding procedure of determining k is not exact but has been found satisfactory. The conductivity k which appears in Eq. (A1.4) corresponds to the temperature T at x = o. The latter differs somewhat from T^* at x = o for the same ΔT. Hence, strictly speaking, k^* should not be taken to equal k in the evaluation of $Q^*_{\ell(h)}$ from Eq. (A1.3). Conceivably, a refined calculation may be desirable for materials which exhibit unusually large variation of k with temperature. This can be done as follows.

---

† The two vertical bars denote absolute values.

Using the procedure heretofore described, a graph which relates conductivity with temperature can be prepared. Values of k^* corresponding to T^* at x = o are read from such graph and improved values of $Q^*_{\ell(h)}$ can thus be calculated from Eq. (A1.3). This should lead to improved values of k. For all tests conducted in the present investigation, such correction amounts to less than 0.5% under the most unfavorable condition.

We now turn to the evaluation of $Q_{\ell(x)}$. To this end, the emittance of the aluminum foil tape which covered the specimen surface must be determined. It was measured in the space simulation chamber with liquid nitrogen cooled shroud. The results of the measurement at three temperatures are given below.

Temperature °R	Total Hemispherical Emittance, ϵ
553	0.070
667	0.069
741	0.071

The small scatter in data is due to experimental errors. A constant value of $\epsilon = 0.07$ was used in all calculations for $Q_{\ell(x)}$.

Interposed between the test specimen at the chamber wall was a radiation shield also of aluminum foil. Its temperatures were not measured, but the mean value could be estimated from a simple heat balance. If we assume that its emittance is identical to that of the aluminum foil tape covering the test specimen, the mean temperature of the radiation shield can be estimated from:

$$\bar{T}_{sh}^{\,4} = \frac{T_w^4 + \frac{A_{sp}}{A_{sh}} \bar{T}_{sp}^{\,4}}{1 + \frac{A_{sp}}{A_{sh}}} \qquad \text{(A1.5)}$$

where the subscripts sh, sp, and w refer respectively to the shield, specimen, and chamber wall. The overscore designates mean values.

The heat loss per unit time over the specimen surface from x = o to

x = x is

$$Q_{\ell(x)} = \epsilon p\sigma \int_0^x (T^4 - \bar{T}_{sh}^4)dx \qquad (A1.6)$$

where ϵ is the emittance, taken to be 0.07 as previously explained, p is the perimeter of the specimen cross section and σ is the Stefan - Boltzmann constant. Inserting Eq. (A1.6) into Eq. (A1.2b) leads to:

$$-kA\frac{dT}{dx} = Q(x) = Q_e - \epsilon p\sigma \int_0^x (T^4 - \bar{T}_{sh}^4)dx \qquad (A1.7)$$

from which values of k corresponding to local temperatures along the length of the specimen can be evaluated. The term involving the integral ranges from less than 1% of Q_e in the case of EC-aluminum specimen to about 4% for 304 stainless steel specimen in the most unfavorable condition. Consequently, one may replace $(T^4 - \bar{T}_{sh}^4)$ by $(\bar{T}^4 - \bar{T}_{sh}^4)$ where $\bar{T}$ is the mean temperature over the length x of the specimen. This resulted in an error of approximately 0.3% at midlength. The local temperature gradients $\frac{dT}{dx}$ in Eq. (A1.7) is evaluated from the derivatives of the computer fitted second degree polynomial for the measured temperatures.

A1.2 Results

The measured values of k of the six metal plates or sheets used in the modeling experimentation for temperatures ranging approximately from 550°R to 800°R are shown in Figs. (A1-4) to (A1-6). All except nickel L exhibit an increase in conductivity with temperature.

A1.3 Error Analysis

The main source of error in the experimental determination of thermal conductivity are due to inaccuracies in the measurement of the following quantities:

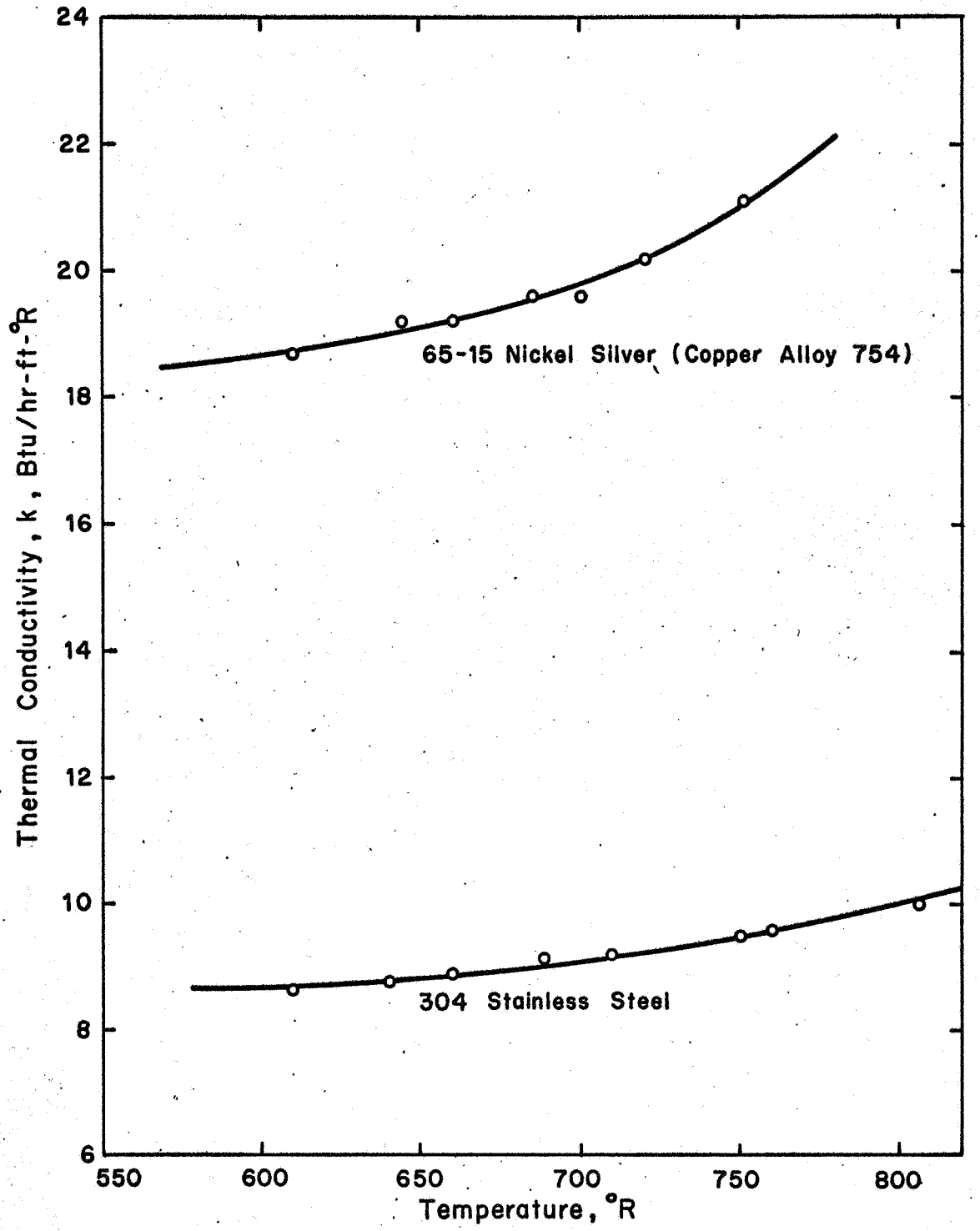

FIG. A 1-4. THERMAL CONDUCTIVITY OF 304 STAINLESS STEEL AND 65-15 NICKEL SILVER.

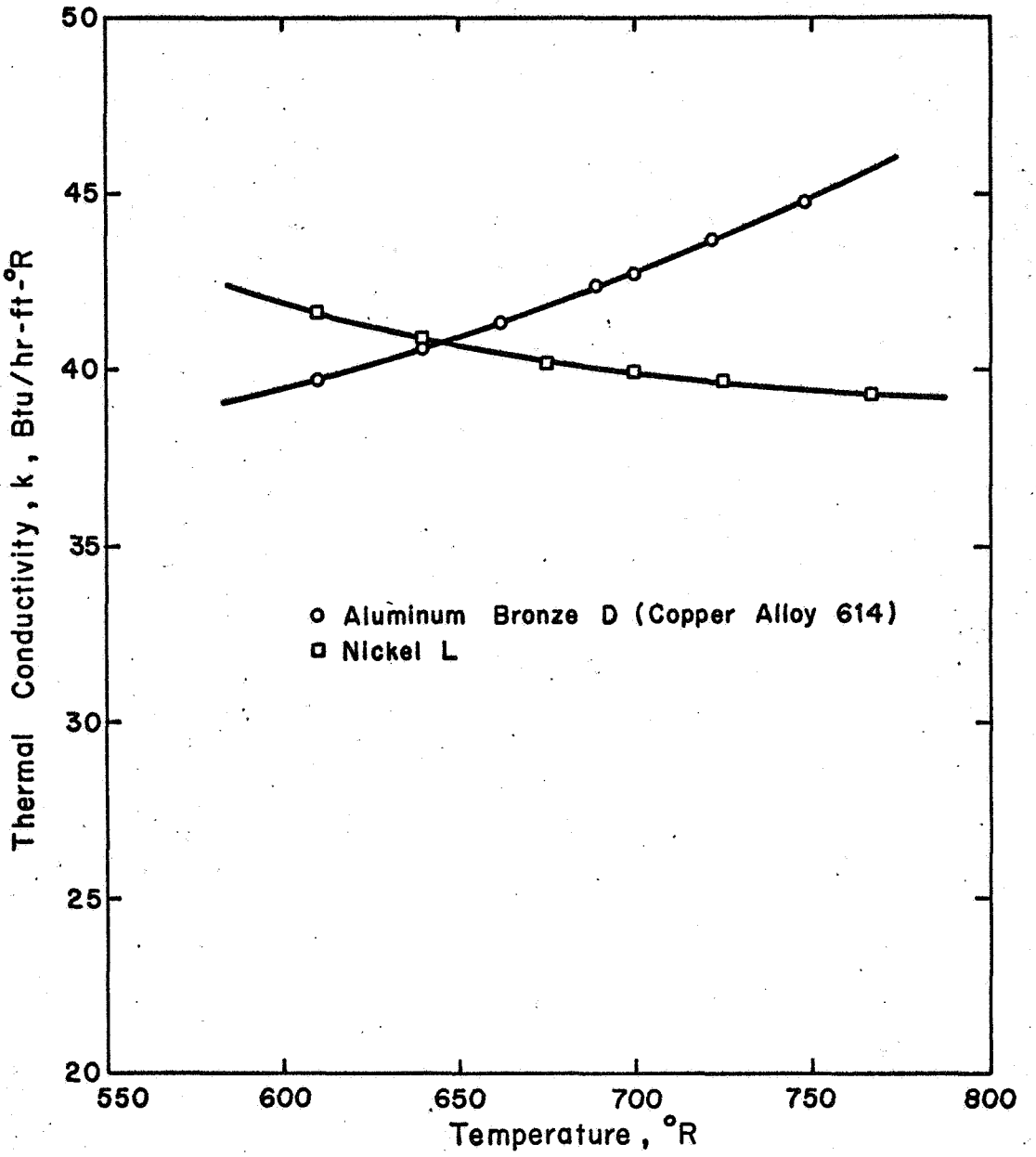

FIG. A 1-5. THERMAL CONDUCTIVITY OF NICKEL L AND ALUMINUM BRONZE D.

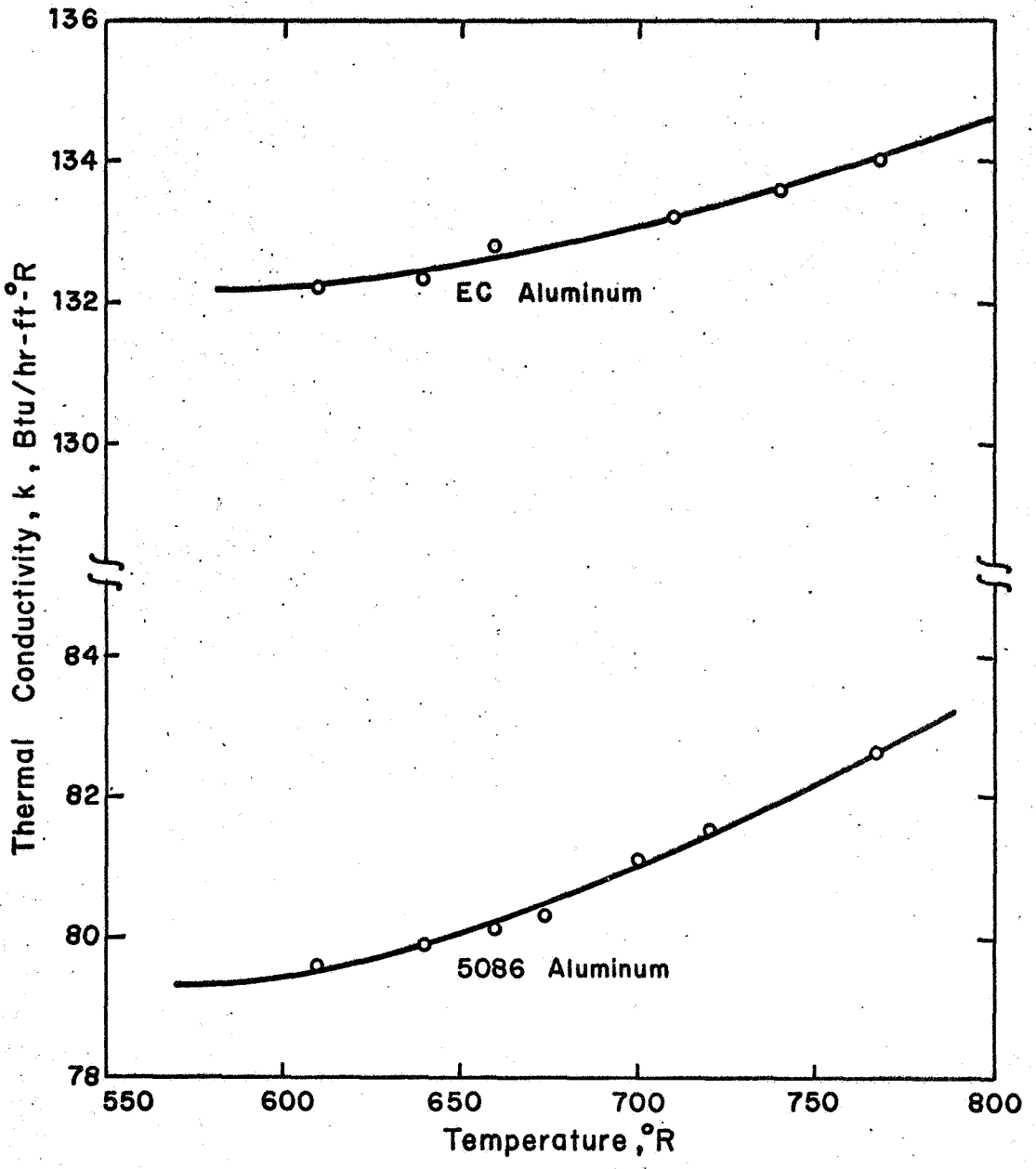

FIG. A1-6. THERMAL CONDUCTIVITY OF 5086 ALUMINUM AND EC ALUMINUM.

(i) heater voltage and current

(ii) local temperatures of the test specimen and thermocouple location

(iii) upper header heat loss and specimen heat loss

(iv) test specimen cross sectional area

For convenient reference, we recapitulate below the equations used in the evaluation of k.

$$Q_e = Q_t - Q_{\ell(h)}. \tag{A1.2b}$$

Under the condition of equal ΔT,

$$Q_{\ell(h)} \doteq Q^*_{\ell(h)} = Q_t^* - k^* A \left|\frac{dT^*}{dx}\right|_{x=o} \tag{A1.3}$$

And,

$$kA \left|\frac{dT}{dx}\right| = Q_e - \epsilon p \sigma \int_o^x (T^4 - \overline{T}_{sh}^4) dx \, . \tag{A1.7}$$

From the first two of the foregoing equations, we obtain

$$Q_e = Q_t - Q_t^* + k^* A \left|\frac{dT^*}{dx}\right|_{x=o} \tag{A1.8}$$

Thence,

$$\left|\frac{\delta Q_e}{Q_e}\right| \le \frac{Q_t}{Q_e}\left|\frac{\delta Q_t}{Q_t}\right| + \frac{Q_t^*}{Q_e}\left|\frac{\delta Q_t^*}{Q_t^*}\right| + \frac{k^* A \left|\frac{dT^*}{dx}\right|_{x=o}}{Q_e}\left\{\left|\frac{\delta k^*}{k^*}\right| + \left|\frac{\delta A}{A}\right| + \left|\frac{\delta\left(\frac{dT^*}{dx}\right)_{x=o}}{\left(\frac{dT^*}{dx}\right)_{x=o}}\right|\right\} \tag{A1.9}$$

Clearly, $$\left|\frac{\delta Q_t}{Q_t}\right| \leq \left|\frac{\delta V}{V}\right| + \left|\frac{\delta I}{I}\right| \qquad \text{(A1.10a)}$$

and $$\left|\frac{\delta Q_t^*}{Q_t^*}\right| \leq \left|\frac{\delta V^*}{V^*}\right| + \left|\frac{\delta I^*}{I^*}\right| \qquad \text{(A1.10b)}$$

wherein V denotes the d.c. potential applied to the heater and I is the corresponding current. Again, quantities with an asterisk refer to those associated with the heat loss test.

From Eq. (A1.7), we may write

$$\frac{\delta\left(kA\left|\frac{dT}{dx}\right|\right)}{kA\left|\frac{dT}{dx}\right|} = \frac{Q_e}{kA\left|\frac{dT}{dx}\right|}\left\{\frac{\delta Q_e}{Q_e} - \frac{\delta Q_{\ell(x)}}{Q_e}\right\} \simeq \left[1 + \frac{Q_{\ell(x)}}{Q_e}\right]\left\{\frac{\delta Q_e}{Q_e} - \frac{Q_{\ell(x)}}{Q_e} \cdot \frac{\delta Q_{\ell(x)}}{Q_{\ell(x)}}\right\} \qquad \text{(A1.11)}$$

where,

$$Q_{\ell(x)} = \epsilon p \sigma \int_0^x (T^4 - \bar{T}_{sh}^4)dx \; . \qquad \text{(A1.6)}$$

The approximation introduced in Eq. (A1.11) is valid since $Q_{\ell(x)} \ll Q_e$. Thus we finally obtain

$$\left|\frac{\delta k}{k}\right| \leq \left[1 + \frac{Q_{\ell(x)}}{Q_e}\right]\left\{\left|\frac{\delta Q_e}{Q_e}\right| + \frac{Q_{\ell(x)}}{Q_e}\left|\frac{\delta Q_{\ell(x)}}{Q_{\ell(x)}}\right|\right\} + \left|\frac{\delta A}{A}\right| + \left|\frac{\delta\left(\frac{dT}{dx}\right)}{\frac{dT}{dx}}\right| \; . \qquad \text{(A1.12)}$$

In Eq. (A1.12), k, $Q_{\ell(x)}$, and $\frac{dT}{dx}$ are local values, the meanings of which have been explained. For our purpose, only estimates of the upper bound of the error and of some representative mean are of interest. The numerical results given below are evaluated in accordance with this viewpoint.

Based on the known or estimated accuracies of the components of the experimental system, the maximum and the probable errors in the various quantities: δV, δI, $\delta\left(\frac{dT}{dx}\right)$, etc., could be appraised. They are listed in

Table A1-1. The error estimates for $\frac{dT^*}{dx}$ and $\frac{dT}{dx}$ were obtained as follows. An uncertainty of 0.2°F in temperature and 0.005 inch in thermocouple location was artificially introduced to one of the nine temperature readings and a least square fit for the temperature distribution by a second degree polynomial was made. From the resulting change in the coefficients of the polynomial, the error in $\frac{dT}{dx}$ could be evaluated. The probable maximum of such errors was assumed to occur when the errors in temperatures and in location of any two adjacent thermocouples were of opposite signs.

Table A1-2 lists the major error sources and their possible contribution to the uncertainties in the measured conductivity values. It is seen that for the experimental system used, the largest error sources were in the measurement of heater voltage and in the evaluation of temperature gradient. An improvement in the former can conceivably be achieved without undue difficulty, while attempts to further reduce errors in $\frac{dT}{dx}$ could not successfully be made without considerable effort and expense.

TABLE A1-1 ESTIMATED MEASUREMENT ERRORS

	$\lvert\delta V\rvert$ (volt)	$\lvert\delta V^*\rvert$ (volt)	$\lvert\delta I\rvert$ (milliamp.)	$\lvert\delta I^*\rvert$ (milliamp.)	$\lvert\delta K^*\rvert$ (Btu/hr-ft-°R)	$\lvert\delta A\rvert$ (sq. in.)	$\delta\left(\frac{dT^*}{dx}\right)_{x=o}$ (°R/ft.)	$\delta\left(\frac{dT}{dx}\right)$ (°R/ft.)	$\delta Q_{\ell(x)}$ (Btu/hr.)
Maximum Error	0.10	0.05	0.40	0.26	0.49	$\sim 10^{-4}$	0.16	0.16	0.13
Probable Error	0.05	0.02	0.20	0.20	0.25	$\sim 10^{-4}$	0.08	0.08	0.10

TABLE A1-2 ESTIMATED ERRORS IN MEASURED CONDUCTIVITY VALUES

Error Source	% Error in k	
	Maximum	Probable
Heater voltage	0.82	0.36
Heater current	0.40	0.30
Test specimen cross-section	~0	~0
Temperature gradient at x=o	0.77	0.38
Upper header heat loss	0.24	0.12
Specimen heat loss	0.19	0.15
Total	2.42	1.31

A1.4 REFERENCES FOR APPENDIX 1

[1] A. Goldsmith, T. E. Waterman, H. J. Hirschhorn, "Handbook of Thermophysical Properties of Solid Materials," Vol. 1 Elements, Vol. 2 Alloys, The Macmillan Company, New York, 1961.

[2] "Thermophysical Properties Research Center Data Book," Vol. 1, Purdue Research Foundation, Indiana, 1966.

[3] "Metal Handbook," Vol. 1, Properties and Selection of Metals, The American Society for Metals, 1961.

[4] "Standards Handbook for Copper and Copper Alloys," 5th Edition, Copper Development Association, Inc., New York, 1964.

[5] "Properties of Some Metals and Alloys," The International Nickel Company, Inc., New York, 1946.

[6] A. M. Clausing, B. T. Chao, "Thermal Contact Resistance in a Vacuum Environment," University of Illinois ME-TN-242-1, 1963.

APPENDIX 2

THERMAL CONDUCTIVITY OF ELECTROPLATED COPPER

The thermal conductivity of electrodeposited copper was determined indirectly. A suitable base metal plate was chosen and its conductivity was measured with and without copper plating. The needed information could then be obtained from (A 2.1) From the consideration of availability and plating requirements, 65 - 15 nickel silver (copper alloy 754) was selected as the base metal. During plating, its orientation with respect to the copper electrode was reversed every 30 minutes to improve the uniformity of the plating thickness. Current density was according to accepted practice.

If we denote the thickness of the nickel silver and that of the electrodeposited copper by d_{NS} and d_{Cu}, and its thermal conductivity without and with copper plating by k_{NS} and k_{NS+Cu}, then

$$k_{Cu} = \frac{k_{NS+Cu}\ (d_{NS} + d_{Cu}) - k_{NS}d_{NS}}{d_{Cu}} \qquad \text{(A 2.1)}$$

where k_{Cu} is the conductivity of the electroplated copper. The two conductivities, k_{NS} and k_{NS+Cu}, were measured by a procedure which had been described in great detail in Appendix 1. The only remaining quantity in (A 2.1) required to be evaluated is d_{Cu}. It was determined as follows:

A short section of about 1/2 inch long was sawed off from the conductivity test specimen and its cross section was polished on a fine emery cloth. The thickness of the copper plating was measured with a Filar microscope head at 20X magnification. Fig. (A2-1) is a photograph taken through a microscope of the nickel silver base plates with electrodeposited copper layers. The epoxy was for cementing the metal plates together to form the conductivity test specimen of desired cross section

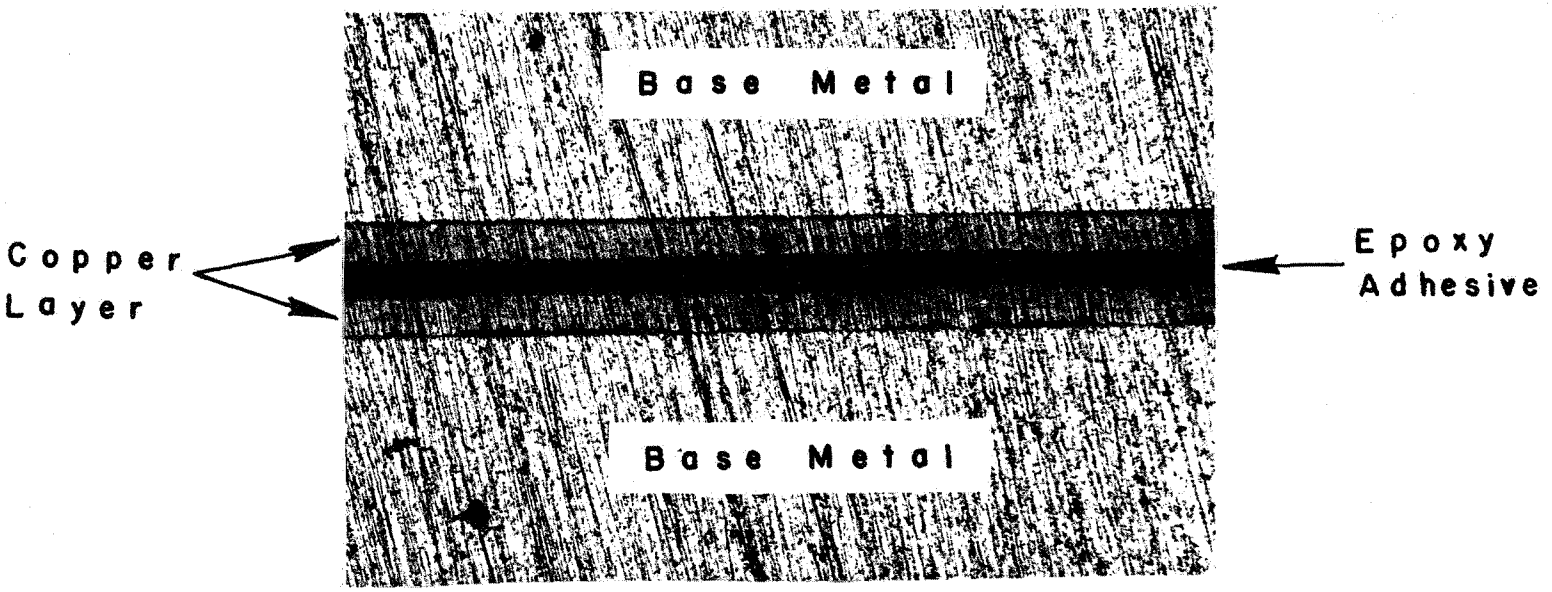

FIG. A2-1 ELECTRODEPOSITED COPPER LAYER ON BASE METAL PLATES

(see Appendix 1). Since the deposited copper is quite soft, the edge adjacent to the epoxy adhesive tends to be smeared by polishing.

The results of measurement are shown plotted in Fig. (A2-2). An error analysis similar to that described in Appendix 1 was made and it was found that the maximum and probable error were about 15% and 8% respectively. The largest error source was the inaccuracies in the thickness determination of the electroplated copper layer. In view of the data shown in Fig. (A2-2) and the relatively large error involved in the measurement, it appears justified to assume that the conductivity of the electrodeposited copper is the same as that of the wrought pure metal.

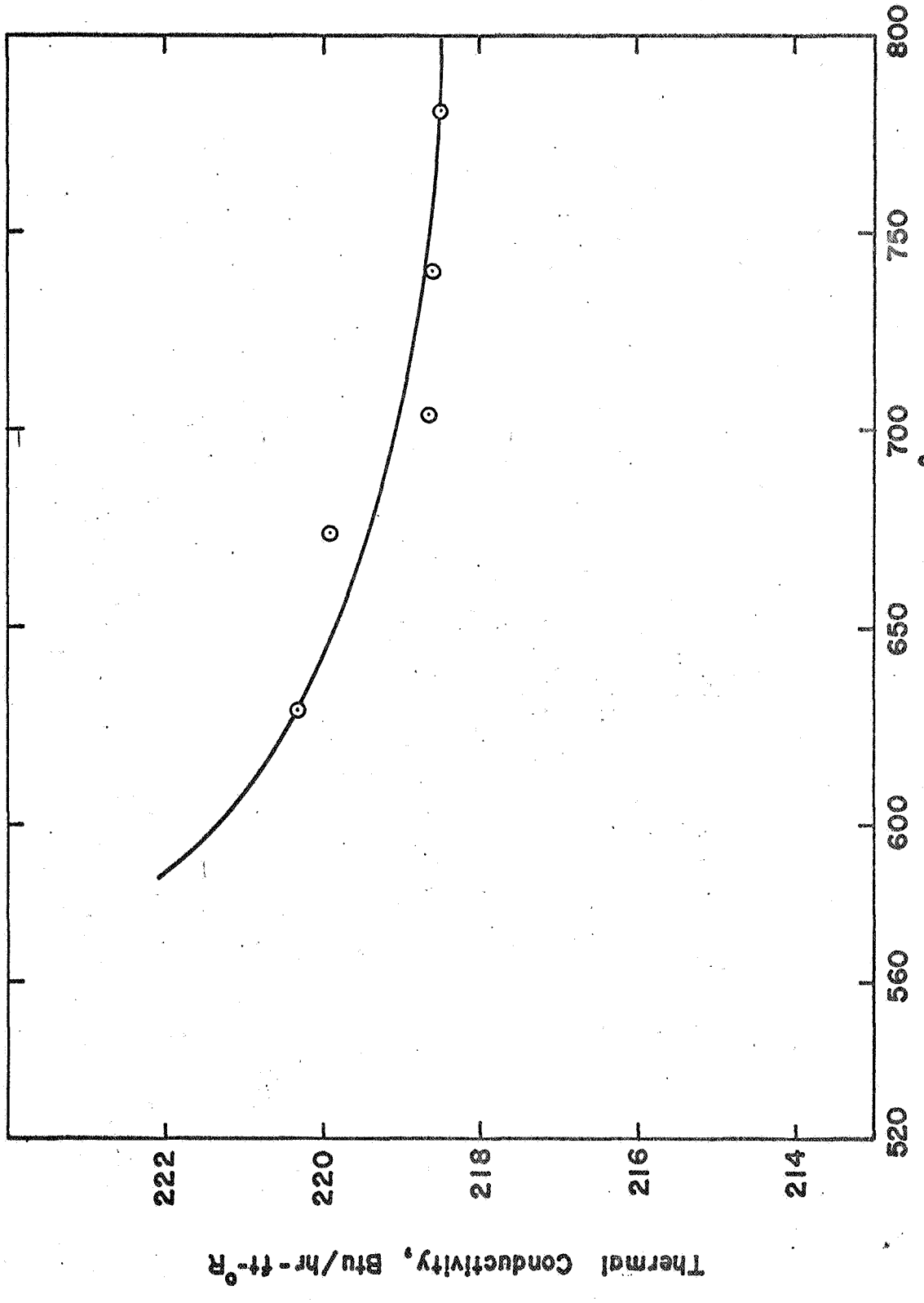

FIG. A2-2 THERMAL CONDUCTIVITY OF ELECTROPLATED COPPER

APPENDIX 3

HEAT CAPACITY DATA

The heat capacities of most elements have been reported over wide temperature ranges. Those of a number of alloys and compounds are also known, at least for room temperatures. Generally speaking reasonable agreement can be found among data published by different investigators. This is in contrast to the observation made for thermal conductivity.

The Thermophysical Properties Research Center of Purdue University kindly provided information for EC-aluminum, nickel L and 304 stainless steel for temperatures ranging from near absolute zero to melting point and beyond. The first two are commercially pure metals and TPRC data agree very well with those given in [1].

The heat capacities of aluminum bronze D (copper alloy No. 614), 5086 aluminum-magnesium alloy, 65-15 nickel silver (copper alloy 754) and 304 stainless steel were calculated by us using the Neumann-Kopp rule. Mr. E. H. Buyco of TPRC also made available to us their computed data for temperatures ranging from 200°K to 600°K (except 304 stainless steel). Our calculated results agree with those of TPRC within 1/2%. In what follows, we briefly describe the procedure used in the computation and the results obtained.

The Neumann-Kopp rule states that the heat capacity of an alloy can be calculated additivelyfrom the heat capacities of its components. This rule is not exact but has been found to be valid for a large number of intermetallic compounds. It holds good especially for alloy phases (See Ref. [2]). To apply the rule the composition and the heat capacity of the elements must be known. Most source books indicate that the molar heat capacity C_p^* of all elements may be represented empirically by an equation of the form:

$$C_p^* = a + bT + cT^{-2} \qquad (A3.1)$$

where a, b and c are constants for a given element and T is the absolute temperature. Reference [1] gives the values of these constants; those for the 8 elements which appear in the 6 materials used in the present modeling experimentation are listed in Table A3-1.

TABLE A3-1 CONSTANTS FOR MOLAR HEAT CAPACITY

$$C_p^* \quad (\text{Cal/mole-degK}) = a + bT + cT^{-2}$$

Element	Atomic Weight	a	$bx10^3$	$cx10^{-5}$	Temperature Range, °K	Accuracy
Al	26.98	4.94	2.96	--	298-mpt	±1%
Cr	52.01	5.84	2.36	-0.88	298-1823	±2%
Cu	63.54	5.41	1.40	--	298-mpt	±1%
Fe(α)	55.85	4.18	5.92	--	298-1000	±2.5%
Mg	24.32	5.33	2.45	-0.103	298-mpt	±1%
Mn(α)	54.94	5.70	3.38	-0.375	298-1000	±1%
Ni(α)	58.71	4.06	7.04	--	298-626	±2%
Zn	65.38	5.35	2.40	--	298-mpt	±1%

As an illustration, let us require to compute the specific heat of aluminum bronze D which has a nominal composition of 91% Cu, 7% Al and 2% Fe. Using the Neumann and Kopp rule, we can write

$$C_p = 0.91 \frac{C_{p,\,Cu}^*}{W_{Cu}} + 0.07 \frac{C_{p,Al}^*}{W_{Al}} + 0.02 \frac{C_{p,Fe}^*}{W_{Fe}} \qquad \text{(A3.2)}$$

where W denotes the atomic weight. Results of calculation are summarized below (C_p in Btu/lb-°R and T in °R):

(1) EC - Aluminun, $\rho = 169$ lb/ft^3

$$C_p = 0.1831 + 0.6095 \times 10^{-4}T$$

(2) Copper, $\rho = 558$ lb/ft^3

$C_p = 0.08514 + 0.1224 \times 10^{-4} T$

(3) Nickel L, $\rho = 555$ lb/ft^3

$C_p = 0.06915 + 0.6662 \times 10^{-4} T$

(4) Aluminum Bronze D (Copper Alloy 614), $\rho = 492.5$ lb/ft^3

$C_p = 0.09179 + 0.1658 \times 10^{-4} T$

(5) 5086 Aluminum, $\rho = 165.9$ lb/ft^3

$C_p = 0.1841 + 0.6060 \times 10^{-4} T - 70.3T^{-2}$

(6) 65-15 Nickel Silver (Copper Alloy 754), $\rho = 542.6$ lb/ft^3

$C_p = 0.08208 + 0.2203 \times 10^{-4} T$

(7) 304 Stainless Steel, $\rho = 494.2$ lb/ft^3

$C_p = 0.07740 + 0.5731 \times 10^{-4} T - 550T^{-2}$

The foregoing results are plotted in Fig. (A3-1) for the temperature range of interest. Their corresponding volumetric heat capacities are shown in Fig. (A3-2).

While our computed data indicated remarkable agreement with those provided by TPRC (probably due to the use of the same source information), one cannot expect that the values shown in the foregoing figures have similar absolute accuracy. Judging from the discussion presented in [1] and [2], it appears reasonable to assume an accuracy of 3 - 4% for the calculated heat capacity values. Another uncertainty is that the composition of the alloys is not precisely known.

REFERENCES FOR APPENDIX 3

[1] C. J. Smithells, "METALS - REFERENCE BOOK, Vol. II", Interscience Publishers Inc., New York and Butterworths Scientific Publications, London, 1955.

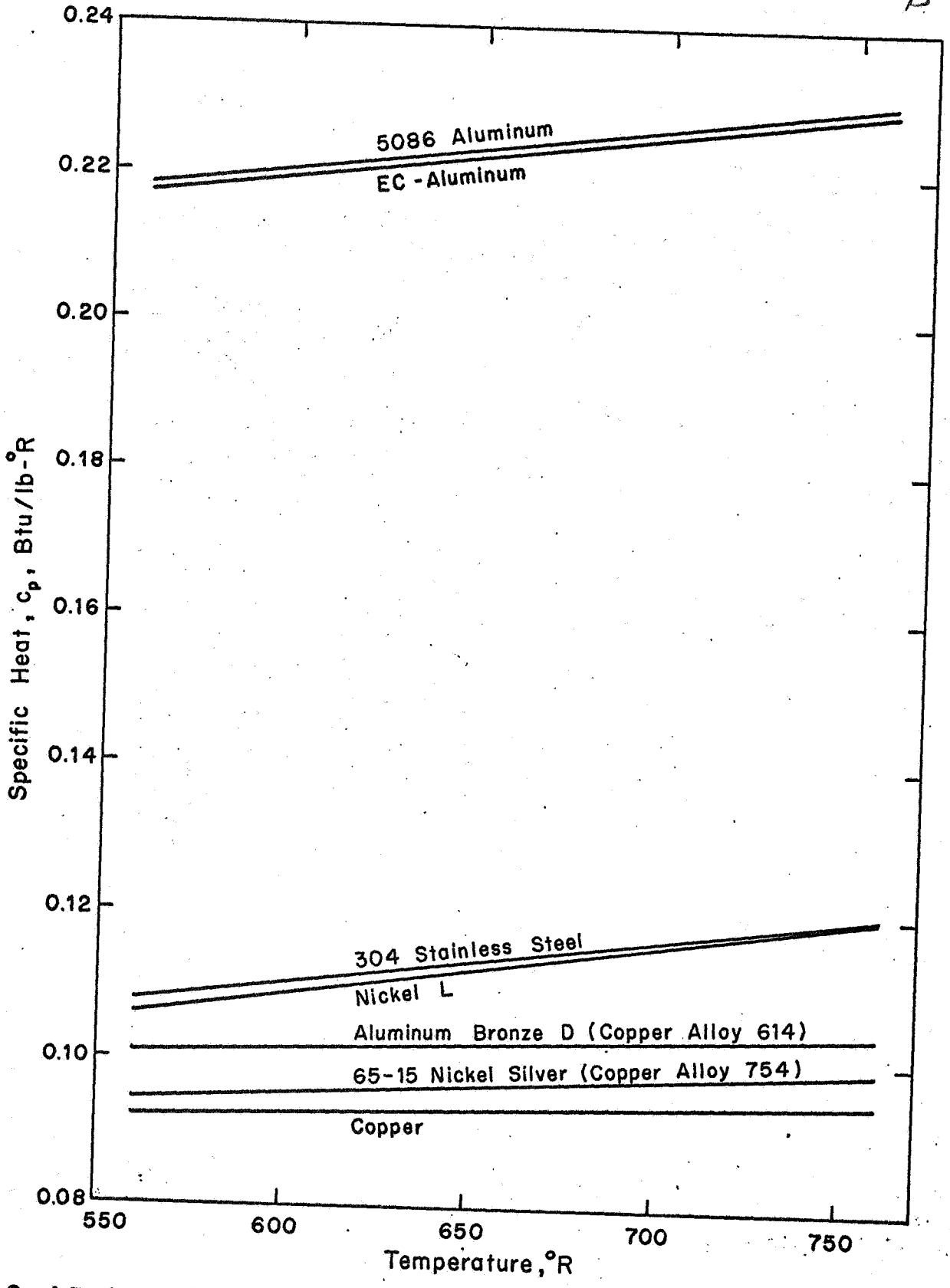

FIG. A3-1. SPECIFIC HEAT OF SEVERAL METALS AND ALLOYS.

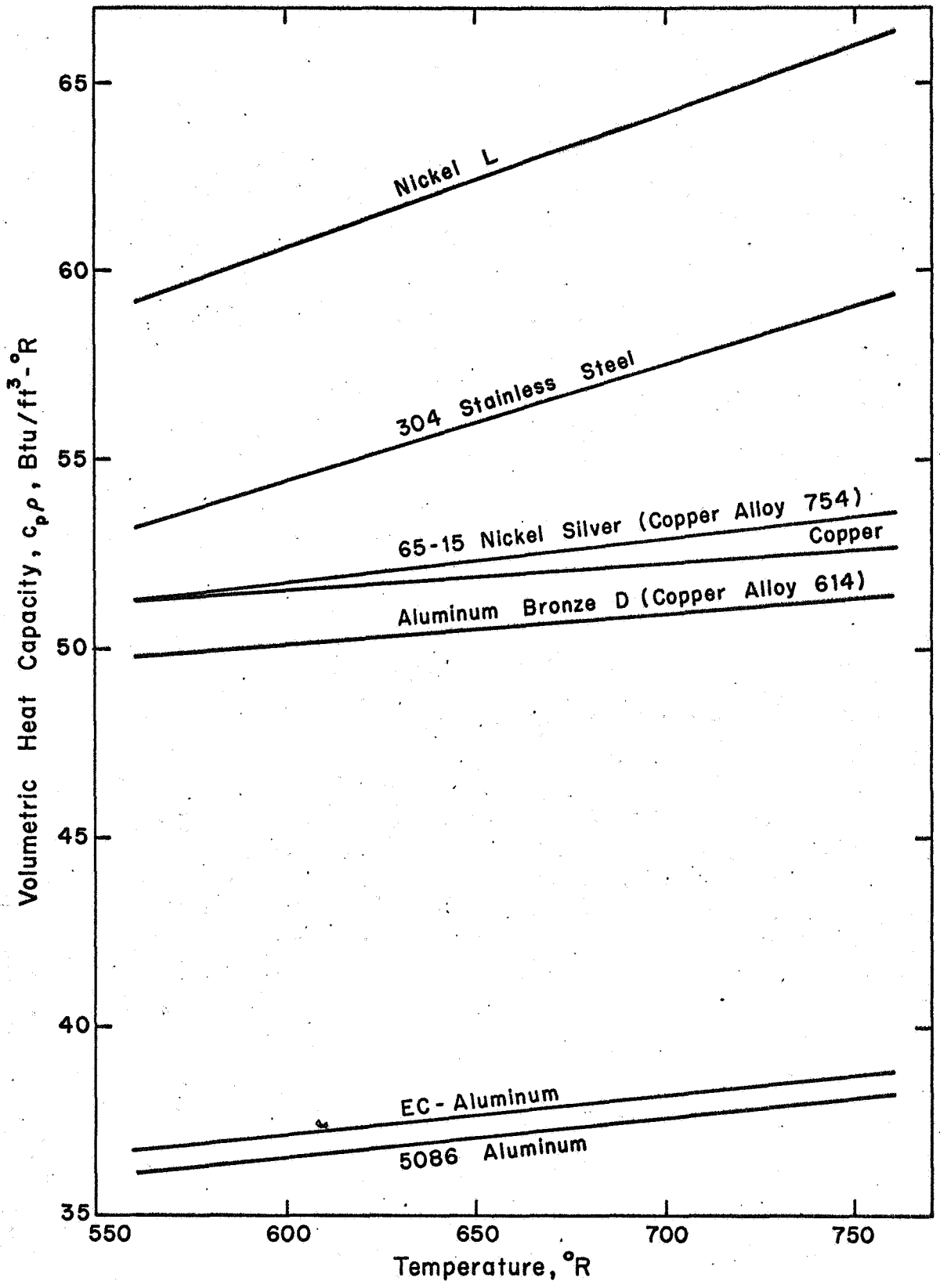

FIG. A3-2. VOLUMETRIC HEAT CAPACITY OF SEVERAL METALS AND ALLOYS.

[2] O. Kubaschewski and E-LL. Evans, "Metallurgical Thermochemistry," Pergamon Press, New York 1958.

APPENDIX 4

THERMOCOUPLE CALIBRATION AND THEIR INSTALLATION PROCEDURE

A4.1 Calibration and Calibration Data

Iron-constantan thermocouples were used throughout in the present investigation.* Three spools, each consisting of 1000 ft of AWG 24,30 and 36 nylon covered solid wires, were acquired from the Thermoelectric Company of New Jersey, They were calibrated for temperatures ranging from room value to slightly above 300°F in an agitated oil bath using the standard procedure. Precision thermometers of three suitable temperature ranges were used as standard. They were all calibrated earlier by the National Bureau of Standards, Washington, D.C. The results of our calibration are summarized in Table A4-1. Based on the calibration data, corrected conversion tables were constructed for each of the three sizes. This was found convenient for temperature evaluation in data processing.

A4.2 Installation Procedure

As stated in Section 4 of this Report, the importance of observing proper installation of thermocouples for temperature measurement of thin sheets like those encountered in the present investigation cannot be overemphasized. Preliminary experimental studies were launched to assess the suitability of several mounting techniques described in the literature. The following procedure has been found most satisfactory and thus adopted.

The thermocouple wires were twisted and beaded, exposing a length of the bare metal slightly shorter than the plate thickness. A hole of

*The thermocouple feedthrough installed in the instrument port of the vacuum chamber and supplied by the AVCO Co. was for iron-constantan couples only.

TABLE A4-1 RESULTS OF THERMOCOUPLE CALIBRATION

AWG 24		AWG 30		AWG 36	
Thermocouple Indicated Temperature °F	Error °F	Thermocouple Indicated Temperature °F	Error °F	Thermocouple Indicated Temperature °F	Error °F
79.3	-0.3	84.8	-0.3	81.8	-0.2
117.1	-0.8	118.9	-0.3	119.0	-0.3
155.4	-0.8	147.5	+0.0	147.8	-0.3
185.1	-0.9	174.3	+0.2	170.3	-0.2
210.2	-0.9	201.4	+0.4	198.3	-0.3
221.9	-0.6	211.8	+0.6	215.7	-0.3
238.5	-0.2	234.0	+0.8	233.0	-0.2
268.7	-0.8	276.1	+1.1	274.9	-0.1
302.9	-0.9	308.9	+1.4	307.6	+0.1

The thermocouple indicated temperature was evaluated from its milivolt output with reference junction at the ice point, using NBS standard conversion tables. A negative error implies that the reading is too low.

diameter slightly greater than the bead was drilled through the plate at the desired location. It was then thoroughly cleaned by rubbing with a commercial solvent, such as GE 1500 thinner. Final cleaning was with methyl alcohol. A high conductivity adhesive cement, Eccobond solder 56C, was mixed with an excess of the recommended liquid catalyst. This 'dilute' cement was rubbed onto the wall of the drilled hole, forming a thin coating. The hole was then filled with the regular cement. The exposed bare metal junction of the thermocouple was cleaned and rubbed with the 'diluted' cement in the same manner. It was then inserted in the hole leaving the nylon insulation just exterior to it. At this position, the tip of the bead should remain completely inside the hole. Excess cement which was squeezed out on that side of the plate where the thermocouple left the surface was gently removed. Curing was done with a hot plate at 150°F to 200°F for about 10 minutes. The excess cement on the other side of the plate was then removed by a razor blade. The plugged hole was carefully inspected at this stage. Occasionally, refilling and recuring were found necessary. Thermocouple beads cemented in this manner cannot be torn apart from the plate without breaking the beads. The thermal paint was sprayed after all the couples were successfully installed. Aluminum foil tape of low surface emittance was applied to that portion of the lead wires at the immediate vicinity of the junction, covering a length of approximately 20 to 30 diameters.

To assess the reliability of thermocouples installed in a manner as above described, two thin, rectangular stainless steel plates with a flat heating element sandwiched in between were fabricated. One reference thermocouple was placed in an isothermal groove, running crosswise from mid-center line toward the plate edge. The groove containing the thermocouple beads was filled with the cement which, after curing, was filed flat so that a continuous plate surface was reformed. The test thermocouple was installed at approximately 1/2 inch from the reference couple junction and along the isothermal extension of the groove at the opposite half of the plate. The plate temperatures were varied from approximately 100°F to 300°F. In no instance, the test thermocouple indicated temperatures which were deviated more than 0.5°F from the reference couple reading.